applied sciences

MDPI

Article

LMIs-Based LPV Control of Quadrotor with Time-Varying Payload

Azmat Saeed [1,*], Aamer I. Bhatti [1] and Fahad M. Malik [2]

[1] Department of Electrical Engineering, Capital University of Science and Technology, Islamabad 45750, Pakistan
[2] Department of Electrical Engineering, College of Electrical and Mechanical Engineering, National University of Sciences and Technology, Islamabad 44000, Pakistan
* Correspondence: azmt.sk@gmail.com; Tel.: +92-333-971-2492

Abstract: Applications of a quadrotor with payload, particularly for chemical spraying, have increased in recent times. The variation in payload mass over time causes a change in the moments of inertia (MOI). Moreover, large tilt angles are required for fast reference tracking and external disturbance rejection. These variations in plant parameters (i.e., mass and inertia) and large tilt angles can degrade the control scheme's performance and stability. This article proposes a linear matrix inequalities (LMIs)-based linear parameter varying (LPV) control scheme for a quadrotor subject to time-varying mass, time-varying inertia, mass flow rate, and large tilt angles. The control strategy is designed by solving LMIs derived from quadratic $\mathcal{H}_\infty$ performance and D-stability. The robust stability and quadratic $\mathcal{H}_\infty$ performance are assessed by LMIs. The efficacy of the proposed methodology is established using numerical simulations, and its performance is compared to the linear time-invariant (LTI) $\mathcal{H}_\infty$ design with pole placement constraints. The results obtained show that the LPV control scheme gives better tracking performance in the presence of time-varying parameters, noise, and external disturbances without actuator saturation. In comparison to the LTI design technique, the proposed LPV scheme improves the rise time (t_r), settling time (t_s), and mean squared error (MSE) by up to 14%, 15%, and 30%, respectively. Moreover, smooth transitions are observed in the tilt angles and control signals with the LPV scheme, contrary to the LTI controller, which exhibits significant oscillations.

Keywords: time-varying mass; quadrotor position control; LPV control; $\mathcal{H}_\infty$ control; LMIs

Citation: Saeed, A.; Bhatti, A.I.; Malik, F.M. LMIs-Based LPV Control of Quadrotor with Time-Varying Payload. *Appl. Sci.* **2023**, *13*, 6553. https://doi.org/10.3390/app13116553

Academic Editors: Yutaka Ishibashi, Cezary Kownacki and Leszek Ambroziak

Received: 7 March 2023
Revised: 20 May 2023
Accepted: 22 May 2023
Published: 28 May 2023

1. Introduction

Quadrotors are used nowadays for a wide range of applications [1,2]. Among these, crop spraying is a significant one that has resulted in enhanced productivity [3,4]. In such applications, the quadrotor mass and MOI change over time. Such large parameter variations, in addition to the standard features of system dynamics, such as nonlinearities, under-actuation, noise, external disturbances, actuator constraint, etc., make the control system design a challenging problem. The quadrotor with payload (liquid tank) is depicted in Figure 1.

Various control strategies have been developed for standard quadrotors to achieve stability and effective tracking. To tackle the quadrotor's tracking control issue, linear control approaches such as proportional–integral–derivative, linear-quadratic-regulator, and $\mathcal{H}_\infty$ have been proposed [5–9]. The above-mentioned control algorithms are based on local linearization, and the performance of an LTI control scheme deteriorates with deviation from the operating point and can even lead to instability. To overcome the impediments caused by local linearization, LPV approaches have been proposed for the quadrotor. In [10], LPV control scheme was suggested for a quadrotor to handle the large perturbation from the nominal condition. Tilt angles were limited to $\pm\pi/8$ rad. In [11],

the LPV controller was proposed for high-speed maneuvering of a quadrotor that requires large tilt angles. Tilt angles were accounted up to $\pm\pi/3$ rad. In [12], a switched LPV control approach was recommended in order to handle huge attitude angles and external disturbances. The region for roll angle ϕ was considered to $\pm\pi/3$ rad and for pitch angle θ, the region was limited to $\pm\pi/8$ rad. Time-varying mass and time-varying inertia were not taken into consideration in the control strategies outlined above.

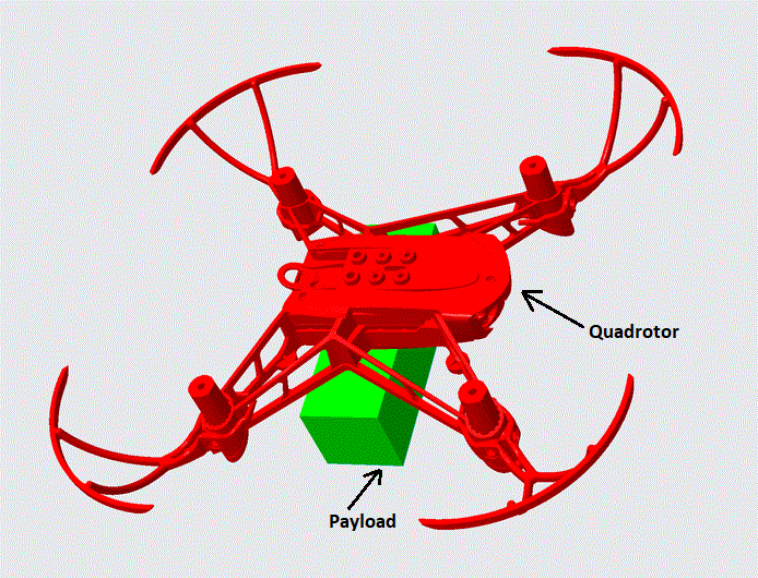

Figure 1. The 3D CAD model of quadrotor with Payload.

The design of the control system for a quadrotor with variable payload has also been investigated in the literature. In [13], LMI-based static output feedback LPV controller was suggested for Attitude/Altitude control of a quadrotor to handle the rotors' velocity variation and step change in mass. The rotors' velocity and mass were assumed to be measurable. Longitudinal and latitudinal translational motions were ignored, and the small angle assumption (i.e., $cos\phi cos\theta \approx 1$) was employed to design the control scheme. Moreover, the mass flow rate was ignored, and the control scheme was conservative due to coupling in the scheduling parameters. In [14], Hybrid LPV control scheme was suggested for the reference tracking of a quadrotor with variable mass and variable inertia. A combination of integral backstepping control and proportional-derivative controls were designed to control the quadrotor's position and altitude. PD controllers were designed using the small angle assumption (i.e., $sin\phi \approx \phi$, $sin\theta \approx \theta$, and $cos\phi \approx cos\theta \approx 1$). Variation in mass was not considered during the control algorithm design. LPV $\mathcal{H}_\infty$ controller was recommended to control the quadrotor rotational dynamics subject to time-varying inertia and variation in the rotors' speed. Mass and rotor speed were considered measurable. The variations in MOI were recalculated in real-time from the changes in the mass. The mass flow rate was not taken into account and the scheduling parameters selected in the proposed scheme did not vary independently, which led to conservative control. A robust LPV $\mathcal{H}_\infty$ controller was proposed for Altitude/Attitude stabilization of a quadrotor to handle mass, inertia, and rotors velocity variations [15]. The proposed controller was designed using the LMI framework. The small angle approximation was considered to design the LPV scheme for the 4 DOF model of the quadrotor. Moreover, position control and the mass flow rate were not taken into consideration, and the coupling in the scheduling parameters led to conservative control. A switched LPV control technique was suggested for the 3 DOF model of a quadrotor subject to large attitude angles, variable inertia, and outside disturbances [16]. Position control dynamics are not considered. In [17], the author recommended a self-tuning PID control scheme for the reference tracking of a quadrotor. Mass and wind disturbance estimators based on a neural network with online learning were suggested

to cope with the system's mass variation and wind disturbances. Variations in MOI due to variable mass and mass flow rate were not taken into consideration. Adaptive sliding mode control (SMC) based on backstepping was advised to reduce the effect of variable load and wind disturbances [18]. Only the changing mass is estimated using the adaptive estimation controller. A fractional SMC was designed to cope with external disturbances and variations in inertia. Actuator limitations and mass flow rate were not considered, and chattering issues existed due to the use of the signum function in the control law. Adaptive non-singular fast terminal SMC was proposed in [19]. External disturbances and mass are estimated online. To address the chattering issue, the saturation function was used in place of the signum function in the control law. Changes in MOI, mass flow rate, and actuator limitation were not taken into consideration. In [20], an adaptive SMC control algorithm was suggested for the quadcopter's altitude tracking in the presence of time-varying payload and ground effect. Position control, MOI variations with mass, and mass flow rate were ignored.

In the LPV control algorithms described in the literature, time-varying mass and large tilt angles have not been considered simultaneously, whereas, in the nonlinear adaptive control schemes suggested for a quadrotor to handle time-varying mass, the controller gains will take time to adapt to the new values. In addition, the computation and execution of gains are online, which will increase the computational burden compared to the LPV approaches, where the gains are computed offline but executed online. The motivation of this paper is to suggest an LMIs-based LPV control scheme for the quadrotor's position control in the presence of time-varying mass, time-varying inertia, mass flow rate, large tilt angles, noise, and external disturbances without actuator saturation.

Contributions

Compared to the prior work, the key contributions of this paper are as follows.

(i) A novel 6 DOF LPV model considering variable mass, variable inertia, mass flow rate, large tilt angles, and wind disturbance is established for the quadrotor.
(ii) The model equations for the variable mass and variable MOI are developed using a curve fitting tool, and a triangle polytope is chosen rather than a rectangular polytope to reduce the number of vertices in the LPV control system. This will reduce the computational load and conservatism of the LPV control strategy.
(iii) LPV control scheme based on LMIs is designed for the LPV model. The robust stability and quadratic $\mathcal{H}_\infty$ performance are assessed by LMIs. The efficacy of the suggested scheme is validated through numerical simulations, and the results are compared with the LTI control scheme.

The rest of the paper is organized as follows. The system dynamic model is presented in Section 2. The steps in the LPV control algorithms are described in Section 3. Section 4 presents the simulation results and their brief descriptions. The paper is concluded in Section 5, followed by the references.

2. System Dynamic Model

A quadrotor is a four-rotor, under-actuated system as depicted in Figure 2. The quadrotor's linear and angular positions are represented by $\begin{bmatrix} x & y & z \end{bmatrix}^T$ and $\begin{bmatrix} \phi & \theta & \psi \end{bmatrix}^T$, respectively. The thrust forces produced by the rotors are represented by $T_i (i = 1, 2, 3, 4)$. The adjacent rotors spin in opposite directions. Two rotors (1 & 3) rotate clockwise, whereas rotors (3 & 4) spin anticlockwise.

A quadrotor with variable payload can be mathematically modeled using the Newton and Euler equations. The quadrotor's translational dynamics with time-varying mass is given by [21,22]

$$\sum F = \frac{d}{dt}(P) = m\frac{d}{dt}(v) + v\frac{d}{dt}(m) \tag{1}$$

where $\sum F$ stands for the resultant force, P represents the linear momentum, m denotes the quadrotor's mass with variable payload, and v indicates the quadrotor's translational velocity.

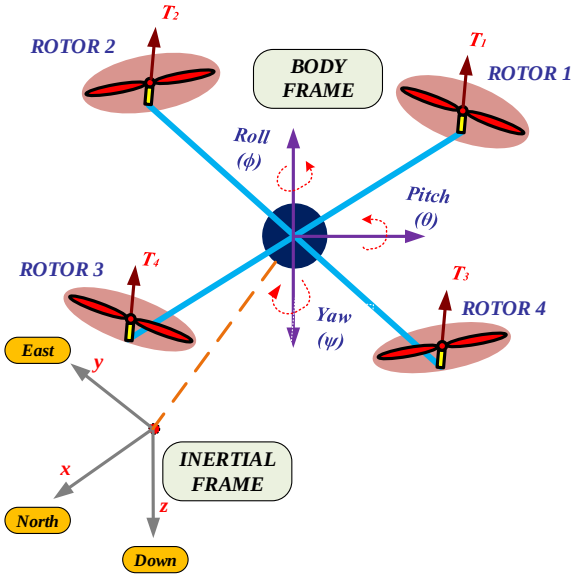

Figure 2. The X-configuration of quadrotor.

Equation (1) can be written as

$$\begin{cases} m\ddot{x} = -(sin\theta cos\phi cos\psi + sin\psi sin\phi)T - \dot{m}\dot{x} - W_{fx} \\ m\ddot{y} = -(cos\phi sin\psi sin\theta - cos\psi sin\phi)T - \dot{m}\dot{y} - W_{fy} \\ m\ddot{z} = -cos\theta cos\phi T + mg - \dot{m}\dot{z} - W_{fz} \end{cases} \tag{2}$$

where

$$T = \sum_{i=1}^{4} T_i = T_1 + T_2 + T_3 + T_4 \tag{3}$$

T represents the thrust force exerted by the rotors, whereas W_{fx}, W_{fy}, and W_{fz} represent the wind forces in x, y, and z directions, respectively.

The wind force can be expressed as [23]

$$\begin{bmatrix} W_{fx} \\ W_{fy} \\ W_{fz} \end{bmatrix} = \begin{bmatrix} k_s|\dot{x} - \dot{x}_w|(\dot{x} - \dot{x_w}) \\ k_s|\dot{y} - \dot{y}_w|(\dot{y} - \dot{y_w}) \\ k_u|\dot{z} - \dot{z}_w|(\dot{z} - \dot{z_w}) \end{bmatrix} \tag{4}$$

$\begin{bmatrix} \dot{x} & \dot{y} & \dot{z} \end{bmatrix}^T$ and $\begin{bmatrix} \dot{x}_w & \dot{y}_w & \dot{z}_w \end{bmatrix}^T$ show the translational and wind velocity, and the parameters k_s and k_u indicate the drag factors on the lower-upper faces and sides of the quadrotor, respectively.

Furthermore, referring to [21,22], the quadrotor's rotational dynamics with time-varying inertia is given by

$$\sum M = J\frac{d}{dt}(\mathcal{W}) + \mathcal{W}\frac{d}{dt}(J) + \mathcal{W} \times J\mathcal{W} \tag{5}$$

where $\sum M$ indicates the net moment, J denotes the inertia tensor, and $\mathcal{W}$ shows the angular speed.

Equation (5) can be written as

$$\begin{cases} I_x\ddot{\phi} = (I_y - I_z)\dot{\theta}\dot{\psi} - \dot{I}_x\dot{\phi} + J_r\Omega_r\dot{\theta} + \tau_\phi \\ I_y\ddot{\theta} = (I_z - I_x)\dot{\psi}\dot{\phi} - \dot{I}_y\dot{\theta} - J_r\Omega_r\dot{\phi} + \tau_\theta \\ I_z\ddot{\psi} = (I_x - I_y)\dot{\phi}\dot{\theta} - \dot{I}_z\dot{\psi} + \tau_\psi \end{cases} \tag{6}$$

where τ_ϕ, τ_θ, and τ_ψ represent the rolling, pitching, and yawning moments, respectively. J_r represents the rotor inertia, $\Omega_r = \Omega_1 + \Omega_3 - \Omega_2 - \Omega_4$, while $\Omega_i (i = 1, 2, 3, 4)$ indicates the speed of rotors.

Control signals are defined for moments and thrust force, which are as follows:

$$\begin{bmatrix} \tau_\phi \\ \tau_\theta \\ \tau_\psi \\ T \end{bmatrix} = \begin{bmatrix} U_1 \\ U_2 \\ U_3 \\ U_4 \end{bmatrix} \tag{7}$$

The relationship between control signals and motor commands is as follows [24,25]:

$$\begin{bmatrix} \cap_1 \\ \cap_2 \\ \cap_3 \\ \cap_4 \end{bmatrix} = \begin{bmatrix} \frac{1}{2\sqrt{2}lK_f} & \frac{1}{2\sqrt{2}lK_f} & -\frac{1}{4K_m} & \frac{1}{4K_f} \\ -\frac{1}{2\sqrt{2}lK_f} & \frac{1}{2\sqrt{2}lK_f} & \frac{1}{4K_m} & \frac{1}{4K_f} \\ -\frac{1}{2\sqrt{2}lK_f} & -\frac{1}{2\sqrt{2}lK_f} & -\frac{1}{4K_m} & \frac{1}{4K_f} \\ \frac{1}{2\sqrt{2}lK_f} & -\frac{1}{2\sqrt{2}lK_f} & \frac{1}{4K_m} & \frac{1}{4K_f} \end{bmatrix} \begin{bmatrix} U_1 \\ U_2 \\ U_3 \\ U_4 \end{bmatrix} \tag{8}$$

where $\cap_i (i = 1, 2, 3, 4)$ represent the squared speed references of the motor (i.e., $\cap_i = \Omega_i^2$).

By combining (2) and (6), the nonlinear 6 DOF model of quadrotor can be written as

$$\begin{cases} I_x\ddot{\phi} = U_1 + (I_y - I_z)\dot{\theta}\dot{\psi} - \dot{I}_x\dot{\phi} + J_r\Omega_r\dot{\theta} \\ I_y\ddot{\theta} = U_2 + (I_z - I_x)\dot{\psi}\dot{\phi} - \dot{I}_y\dot{\theta} - J_r\Omega_r\dot{\phi} \\ I_z\ddot{\psi} = U_3 + (I_x - I_y)\dot{\phi}\dot{\theta} - \dot{I}_z\dot{\psi} \\ m\ddot{x} = -(sin\theta cos\phi cos\psi + sin\psi sin\phi)U_4 - \dot{m}\dot{x} - W_{fx} \\ m\ddot{y} = -(cos\phi sin\psi sin\theta - cos\psi sin\phi)U_4 - \dot{m}\dot{y} - W_{fy} \\ m\ddot{z} = -cos\theta cos\phi U_4 - \dot{m}\dot{z} + mg - W_{fz} \end{cases} \tag{9}$$

Table 1 shows the quadrotor's parameters with full payload.

Table 1. Quadrotor parameters with full payload.

Quantity	Symbol	Value	Unit
Mass of quadrotor	$\overline{\mathrm{m}}$	1.0497×10^{-1}	kg
Inertia about the x-axis	$\overline{\mathrm{I_x}}$	1.1568×10^{-4}	kg m^2
Inertia about the y-axis	$\overline{\mathrm{I_y}}$	1.1378×10^{-4}	kg m^2
Inertia about the z-axis	$\overline{\mathrm{I_z}}$	1.2595×10^{-4}	kg m^2
Length of an arm	l	6.24×10^{-2}	m
Rotor inertia	$\mathrm{J_r}$	1.4338×10^{-4}	kg m^2
Drag factor	k_s	2.8×10^{-2}	kg/m
Drag factor	k_u	5.4×10^{-2}	kg/m
Thrust coefficient	K_f	6.5330×10^{-4}	N/(rad^2/s^2)
Thrust coefficient	K_m	1.5769×10^{-6}	Nm/(rad^2/s^2)
Acceleration of gravity	g	9.81	m/s^2

Variation in the System's Mass and Moments of Inertia Parameters

To develop the model equations for time-varying mass and time-varying inertia, we have used SOLIDWORKS. The 3D CAD (three-dimensional computer-aided design) model of the quadrotor with payload developed in SOLIDWORKS is shown in Figure 1. The mass and MOI values are noted at different levels of the water in the liquid tank. The values recorded are listed in Table 2. The curve fitting toolbox available in MATLAB was used to find the model equations for mass and MOI. The root mean squared error ($RMSE$) was used to assess the goodness of fit. The variation in the values of the system's mass and MOI are shown in Figures 3 and 4.

Table 2. Mass and inertia values at different water levels.

S.No	Water Level (m)	Mass (kg)	I_x (kg m^2)	I_y (kg m^2)	I_z (kg m^2)
1	1.71×10^{-2}	1.0497×10^{-1}	1.1568×10^{-4}	1.1378×10^{-4}	1.2595×10^{-4}
2	1.52×10^{-2}	1.0141×10^{-1}	1.1311×10^{-4}	1.1254×10^{-4}	1.2396×10^{-4}
3	1.33×10^{-2}	9.7844×10^{-2}	1.1022×10^{-4}	1.1099×10^{-4}	1.2196×10^{-4}
4	1.14×10^{-2}	9.4281×10^{-2}	1.0697×10^{-4}	1.0906×10^{-4}	1.1994×10^{-4}
5	9.47×10^{-3}	9.0756×10^{-2}	1.0331×10^{-4}	1.067×10^{-4}	1.1794×10^{-4}
6	7.57×10^{-3}	8.7194×10^{-2}	9.910×10^{-5}	1.0380×10^{-4}	1.1590×10^{-4}
7	5.68×10^{-3}	8.3650×10^{-2}	9.431×10^{-5}	1.0028×10^{-4}	1.1386×10^{-4}
8	3.78×10^{-3}	8.0088×10^{-2}	8.876×10^{-5}	9.601×10^{-5}	1.1179×10^{-4}
9	1.86×10^{-3}	7.6488×10^{-2}	8.230×10^{-5}	9.080×10^{-5}	1.0967×10^{-4}
10	0	7.3002×10^{-2}	7.506×10^{-5}	8.477×10^{-5}	1.0760×10^{-4}

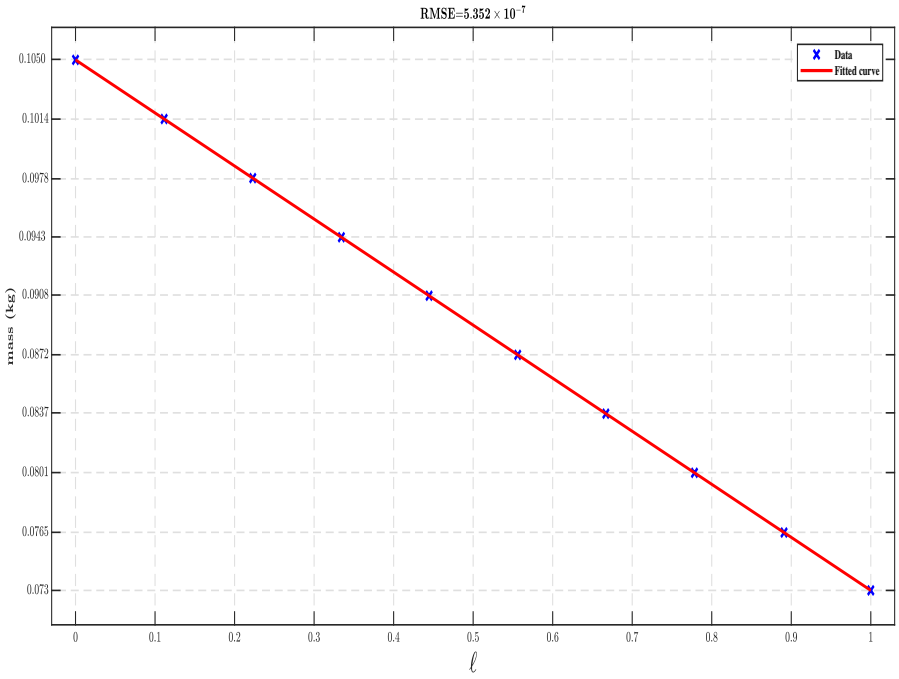

Figure 3. Variation in mass with parameter ℓ.

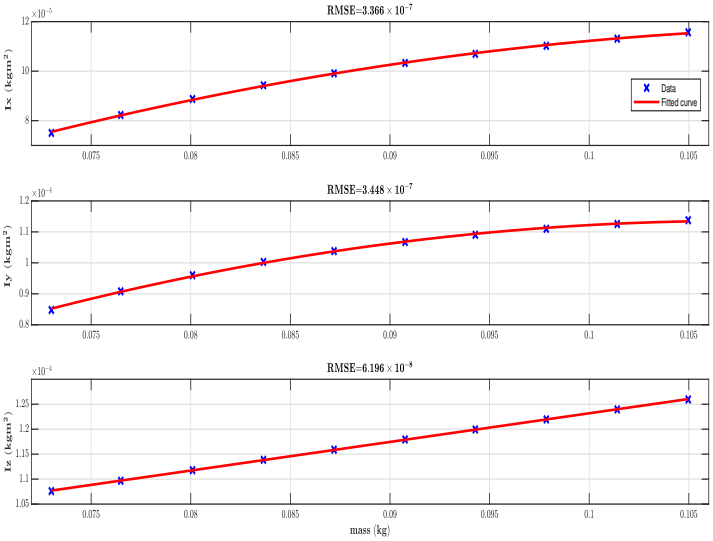

Figure 4. Variation in MOI with mass.

A parameter ℓ has been introduced which is given as:

$$\ell = \frac{\overline{h} - h}{\overline{h}} \tag{10}$$

where h represents the level of the water in the tank and $\overline{h}$ indicates the water level when the payload is filled to capacity.

The equations of the mass and MOI obtained using curve fitting are:

$$\begin{cases} m = a_1\ell + a_2 \\ I_x = b_1m^2 + b_2m + b_3 \\ I_y = c_1m^2 + c_2m + c_3 \\ I_z = d_1m + d_2 \end{cases} \tag{11}$$

The derivatives are:

$$\begin{cases} \dot{m} = a_1\dot{\ell} \\ \dot{I}_x = 2b_1m\dot{m} + b_2\dot{m} \\ \dot{I}_y = 2c_1m\dot{m} + c_2\dot{m} \\ \dot{I}_z = d_1\dot{m} \end{cases} \tag{12}$$

Table 3 shows the parameter values in Equation (11).

Table 3. Parameter values.

Parameter	Value	Unit
a_1	-3.1967×10^{-2}	kg
a_2	1.0501×10^{-1}	kg
b_1	-2.3181×10^{-2}	m^2/kg
b_2	5.3709×10^{-3}	m^2
b_3	-1.9308×10^{-4}	kg m^2
c_1	-2.3731×10^{-2}	m^2/kg
c_2	5.1061×10^{-3}	m^2
c_3	-1.6102×10^{-4}	kg m^2
d_1	5.7349×10^{-4}	m^2
d_2	6.5828×10^{-5}	kg m^2

The LPV model for a dynamic system is not unique. Multiple LPV models can exist for a dynamic system. The time-varying parameters chosen in the LPV model determine the complexity and effectiveness of the control system. The following assumptions are taken into account in order to establish an affine LPV model of quadrotor with time-varying payload [11,16].

- The sine and cosine of tilt angles are approximated by the second-order Taylor's expansion.
- The input $U_4 \approx mg$, $sin\psi \approx 0$, and $cos\psi \approx 1$ are considered to make the dependency between system states $\left(i.e., \begin{bmatrix} x & y \end{bmatrix}^T on \begin{bmatrix} \phi & \theta \end{bmatrix}^T\right)$ explicitly.

Using the above assumptions, and considering the small gyro effect, the simplified nonlinear model is obtained, which is as follows:

$$\begin{cases} I_x\ddot{\phi} = U_1 - \dot{I}_x\dot{\phi} \\ I_y\ddot{\theta} = U_2 - \dot{I}_y\dot{\theta} \\ I_z\ddot{\psi} = U_3 - \dot{I}_z\dot{\psi} \\ \ddot{x} = -\left(\theta - \dfrac{\theta^3}{6}\right)\left(1 - \dfrac{\phi^2}{2}\right)g - \dfrac{\dot{m}}{m}\dot{x} - \dfrac{W_{fx}}{m} \\ \ddot{y} = \left(\phi - \dfrac{\phi^3}{6}\right)g - \dfrac{\dot{m}}{m}\dot{y} - \dfrac{W_{fy}}{m} \\ m\ddot{z} = -\left(1 - \dfrac{\theta^2}{2}\right)\left(1 - \dfrac{\phi^2}{2}\right)(mg + u_4) + mg - \dot{m}\dot{z} - W_{fz} \end{cases} \tag{13}$$

By using Equations (11)–(13), the LPV model of the quadrotor is obtained, which is given as

$$\begin{cases} (b_1\rho_1 + b_2 + b_3\rho_2)\ddot{\phi} = \rho_2 U_1 - (2b_1\dot{\phi} + b_2\rho_2\dot{\phi})d_r \\ (c_1\rho_1 + c_2 + c_3\rho_2)\ddot{\theta} = \rho_2 U_2 - \left(2c_1\dot{\theta} + c_2\rho_2\dot{\theta}\right)d_r \\ (d_1\rho_1 + d_2)\ddot{\psi} = U_3 - d_1 d_r\dot{\psi} \\ \ddot{x} = -g\theta + \dfrac{g}{2}\rho_3\theta + \dfrac{g}{6}\rho_4\theta - d_r\rho_2\dot{x} - \rho_2 d_x \\ \ddot{y} = g\phi - \dfrac{g}{6}\rho_3\phi - d_r\rho_2\dot{y} - \rho_2 d_y \\ \rho_1\ddot{z} = \dfrac{1}{2}\rho_3 u_4 + \dfrac{1}{2}\rho_4 u_4 - u_4 - d_r\dot{z} - d_z \end{cases} \tag{14}$$

where $\rho = [\rho_1 \ \rho_2 \ \rho_3 \ \rho_4]^T$ is a time-varying parameters vector. The terms $\dfrac{\phi^2\theta^2}{4}$ and $\dfrac{\phi^2\theta^3}{12}$ are neglected because of their high power and relatively modest contribution. $\begin{bmatrix} d_x & d_y & d_z & d_r \end{bmatrix}^T$ denote the bounded disturbances and are given as

$$\begin{cases} d_x = W_{fx} \\ d_y = W_{fy} \\ d_z = W_{fz} - \dfrac{mg\phi^2}{2} - \dfrac{mg\theta^2}{2} \\ d_r = \dot{m} \end{cases} \tag{15}$$

The scheduling parameters of the LPV model are

$$\begin{aligned} \rho_1 &= m\,\epsilon\begin{bmatrix} 1.05 \times 10^{-1} & 7.3 \times 10^{-2} \end{bmatrix} = \begin{bmatrix} \overline{\rho_1} & \underline{\rho_1} \end{bmatrix} \\ \rho_2 &= \frac{1}{m}\,\epsilon\begin{bmatrix} 1.371 \times 10^{1} & 9.51 \times 10^{0} \end{bmatrix} = \begin{bmatrix} \overline{\rho_2} & \underline{\rho_2} \end{bmatrix} \\ \rho_3 &= \phi^2\,\epsilon\begin{bmatrix} (\frac{\pi}{3})^2 & 0 \end{bmatrix} = \begin{bmatrix} \overline{\rho_3} & \underline{\rho_3} \end{bmatrix} \\ \rho_4 &= \theta^2\,\epsilon\begin{bmatrix} (\frac{\pi}{3})^2 & 0 \end{bmatrix} = \begin{bmatrix} \overline{\rho_4} & \underline{\rho_4} \end{bmatrix} \end{aligned}$$

where the units of mass and angles are kg and rad, respectively.

3. LPV Control Design

In this section, we present an LMIs-based LPV control design for position tracking of the quadrotor. The goal is that the state variables $[x, \ y, \ z]$ follow the desired reference trajectories $[x_{ref}, \ y_{ref}, \ z_{ref}]$, while the yaw angle ψ is required to remain at $\angle 0^0$. All the state variables $[x, \ y, \ z, \ \phi, \ \theta, \ \psi, \ \dot{\phi}, \ \dot{\theta}, \ \dot{\psi}, \ \dot{x}, \ \dot{y}, \ \dot{z}]$ and the water level in the liquid tank are considered as measurable. Based on the system dynamics, the control system is split into subsystems.

(1) The fully actuated subsystem dynamics that consist of $\ddot{z}$ and $\ddot{\psi}$.
(2) The under-actuated subsystem dynamics made up of $\ddot{\phi}$, $\ddot{\theta}$, $\ddot{x}$, and $\ddot{y}$.

The LPV control system configuration is depicted in Figure 5. $P(\rho)$ shows the generalized LPV plant and $K(\rho)$ depicts the LPV controller gains.

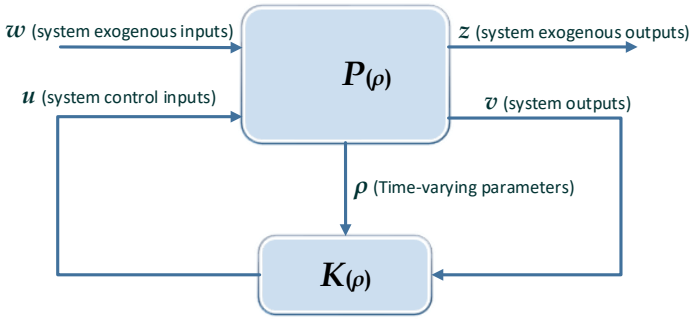

Figure 5. The structure of closed-loop LPV system.

The generalized LPV plant's state-space realization is as follows [26,27]:

$$\begin{cases} \dot{\chi} = \mathcal{A}(\rho)\chi + \mathcal{B}_1(\rho)w + \mathcal{B}_2(\rho)u \\ z = \mathcal{C}_z(\rho)\chi + \mathcal{D}_{11}(\rho)w + \mathcal{D}_{12}(\rho)u \\ v = \mathcal{C}_v(\rho)\chi + \mathcal{D}_{21}(\rho)w + \mathcal{D}_{22}(\rho)u \end{cases} \tag{16}$$

where

(1) $\chi \in R^n$, $w \in R^{n_w}$, $u \in R^{n_u}$, $z \in R^{n_z}$ and $v \in R^{n_v}$ are the system states, exogenous inputs (i.e., reference signals and disturbances), control signals, exogenous outputs, and sensed outputs, respectively.

(2) $\mathcal{A}(\rho)$, $\mathcal{B}_1(\rho)$, $\mathcal{B}_2(\rho)$, $\mathcal{C}_z(\rho)$, $\mathcal{D}_{11}(\rho)$, $\mathcal{D}_{12}(\rho)$, $\mathcal{C}_v(\rho)$, $\mathcal{D}_{21}(\rho)$ and $\mathcal{D}_{22}(\rho)$ are parameter dependent state-space matrices of appropriate dimensions.

(3) ρ is a time-varying parameters vector that varies in a convex polytope of vertices $\rho_{vi}(i = 1, 2, \ldots, N)$. N represents the number of vertices.

The LPV control law is given as:

$$u(t) = K(\rho)v(t) \tag{17}$$

In the LPV polytopic form, the matrices of $P(\rho)$ can be written as

$$\begin{bmatrix} \mathcal{A}(\rho) & \mathcal{B}_1(\rho) & \mathcal{B}_2(\rho) \\ \mathcal{C}_z(\rho) & \mathcal{D}_{11}(\rho) & \mathcal{D}_{12}(\rho) \\ \mathcal{C}_v(\rho) & \mathcal{D}_{21}(\rho) & \mathcal{D}_{22}(\rho) \end{bmatrix} = \sum_{i=1}^{N} \alpha_i \begin{bmatrix} A_i & B_{1i} & B_{2i} \\ C_{zi} & D_{11i} & D_{12i} \\ C_{vi} & D_{21i} & D_{22i} \end{bmatrix} \tag{18}$$

In the polytopic form, LPV controller gains $K(\rho)$ can be expressed as

$$K(\rho) = \sum_{i=1}^{N} \alpha_i K_i \tag{19}$$

$\alpha_i(i = 1, 2, \ldots, N)$ represent the barycentric weights (for details, see [28,29]). The time-varying parameter vector ρ can be expressed as

$$\rho = \left\{ \alpha_i \rho_{vi}, \quad \alpha_i \geq 0, \quad \textstyle\sum_{i=1}^{N} \alpha_i = 1 \right\}$$

To design an LPV controller, a mixed sensitivity control approach is adopted [30,31]. The weighted closed-loop system for mixed sensitivity control design is shown in Figure 6.

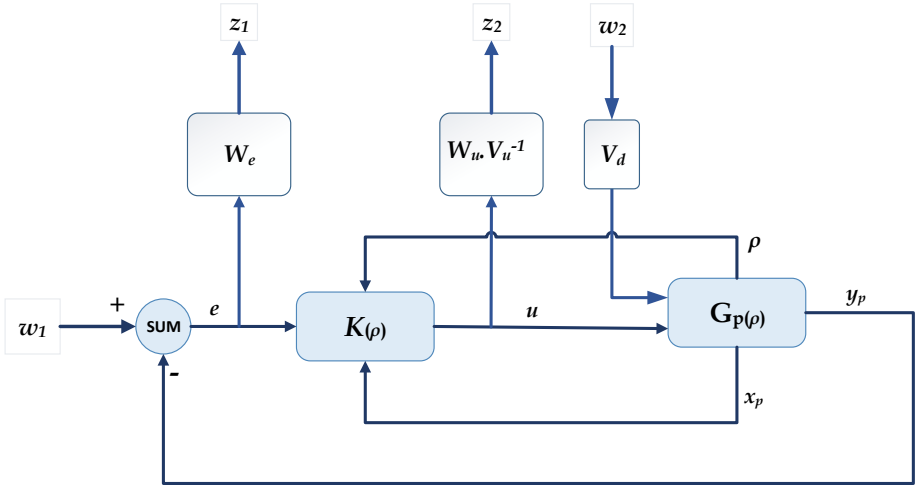

Figure 6. The mixed sensitivity control problem.

$G_P(\rho)$ shows the LPV model of the dynamic system to the control signal u and the disturbance signal w_2, W_e is the weighting filter that is chosen to impose meaningful requirements on the closed-loop system, such as trajectory tracking and disturbance rejection, V_u and V_d are the static weights that represent the maximum values of control signal and disturbance signal, respectively.

The state-space realization of $G_P(\rho)$ and W_e is given by

$$\left[\begin{array}{c} \dot{x}_p \\ \hline y_p \end{array}\right] = \left[\begin{array}{c|cc} A_p(\rho) & B_w(\rho)V_d & B_p(\rho) \\ \hline C_p(\rho) & 0 & 0 \end{array}\right] \left[\begin{array}{c} x_p \\ w_2 \\ u \end{array}\right] \tag{20}$$

$$\left[\begin{array}{c} \dot{x}_{We} \\ \hline z_1 \end{array}\right] = \left[\begin{array}{c|c} A_{We} & B_{We} \\ \hline C_{We} & D_{We} \end{array}\right] \left[\begin{array}{c} x_{We} \\ \hline e \end{array}\right] \tag{21}$$

The state-space realization for LPV controller synthesis is given as:

$$\left[\begin{array}{c} \dot{x}_p \\ \dot{x}_{We} \\ \hline z_1 \\ z_2 \end{array}\right] = \left[\begin{array}{cc|ccc} A_p(\rho) & 0 & 0 & B_w(\rho)V_d & B_p(\rho)V_u \\ -B_{We}C_p(\rho) & A_{We} & B_{We} & 0 & 0 \\ \hline -D_{We}C_p(\rho) & C_{We} & D_{We} & 0 & 0 \\ 0 & 0 & 0 & 0 & 1 \end{array}\right] \left[\begin{array}{c} x_p \\ x_{We} \\ \hline w_1 \\ w_2 \\ \hat{u} \end{array}\right] \tag{22}$$

The scaled control input $\hat{u}$ is given by

$$\hat{u} = V_u^{-1}u \tag{23}$$

The LPV controller is designed using the following well-known lemmas, which describe the $\mathcal{H}_\infty$-norm and regional pole placement in the LMI region [32,33].

Lemma 1. *$\mathcal{H}_\infty$-norm*

The $\mathcal{H}_\infty$-norm of closed-loop LPV system from exogenous inputs w to exogenous outputs z will be lower than a positive scalar γ, if and only if there exists a positive-definite symmetric matrix $X(\rho)$, and a matrix $Y(\rho)$ for all the admissible values of time-varying parameter vector ρ satisfying

$$\begin{cases} min & \gamma \\ s.t. & X(\rho) > 0 \\ & \begin{bmatrix} \mathcal{A}(\rho)X(\rho) + X(\rho)\mathcal{A}(\rho)^T + \mathcal{B}_2(\rho)Y(\rho) + Y(\rho)^T\mathcal{B}_2(\rho)^T & \mathcal{B}_1(\rho) & X(\rho)\mathcal{C}_z(\rho)^T + Y(\rho)^T\mathcal{D}_{12}(\rho)^T \\ \mathcal{B}_1(\rho)^T & -\gamma I & \mathcal{D}_{11}(\rho)^T \\ \mathcal{C}_z(\rho)X(\rho) + \mathcal{D}_{12}(\rho)Y(\rho) & \mathcal{D}_{11}(\rho) & -\gamma I \end{bmatrix} < 0 \end{cases} \tag{24}$$

Lemma 2. *Regional pole constraints*

The closed-loop LPV system's eigenvalues will be located in the desirable LMI region $D_{(\alpha,\beta,\varphi)}$*, if and only if there exist* $X(\rho)$*, and* $Y(\rho)$*, such that*

$$\begin{cases} X(\rho) > 0 \\ 2\alpha X(\rho) + \mathcal{A}(\rho)X(\rho) + \mathcal{B}_2(\rho)Y(\rho) + X(\rho)\mathcal{A}(\rho)^T + Y(\rho)^T\mathcal{B}_2(\rho)^T < 0 \\ 2\beta X(\rho) + \mathcal{A}(\rho)X(\rho) + \mathcal{B}_2(\rho)Y(\rho) + X(\rho)\mathcal{A}(\rho)^T + Y(\rho)^T\mathcal{B}_2(\rho)^T > 0 \end{cases} \tag{25}$$

and

$$\begin{bmatrix} \left(X(\rho)\mathcal{A}(\rho)^T + \mathcal{A}(\rho)X(\rho) + Y(\rho)^T\mathcal{B}_2(\rho)^T + \mathcal{B}_2(\rho)Y(\rho)\right)sin\varphi & \left(X(\rho)\mathcal{A}(\rho)^T - \mathcal{A}(\rho)X(\rho) - \mathcal{B}_2(\rho)Y(\rho) + Y(\rho)^T\mathcal{B}_2(\rho)^T\right)cos\varphi \\ \left(\mathcal{A}(\rho)X(\rho) - X(\rho)\mathcal{A}(\rho)^T + \mathcal{B}_2(\rho)Y(\rho) - Y(\rho)^T\mathcal{B}_2(\rho)^T\right)cos\varphi & \left(\mathcal{A}(\rho)X(\rho) + X(\rho)\mathcal{A}(\rho)^T + \mathcal{B}_2(\rho)Y(\rho) + Y(\rho)^T\mathcal{B}_2(\rho)^T\right)sin\varphi \end{bmatrix} < 0 \tag{26}$$

where the LMI region $D_{(\alpha,\beta,\varphi)} = D_{(\alpha,\beta)} \cap D_{(\varphi)}$*. The system will be D-stable if both conditions* (25) *and* (26) *are satisfied. The sub-LMI regions* $D_{(\alpha,\beta)}$ *and* $D_{(\varphi)}$ *are shown in Figures 7 and 8.*

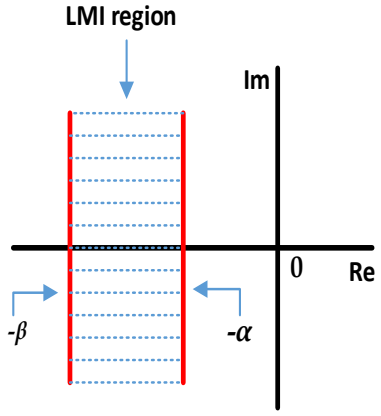

Figure 7. Strip region $D_{(\alpha,\beta)}$.

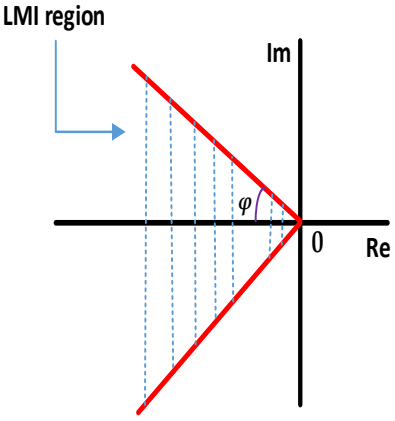

Figure 8. Conic sector $D_{(\varphi)}$.

The LPV controller gains $K(\rho)$ can be determined as follows:

$$K(\rho) = Y(\rho)X(\rho)^{-1} \tag{27}$$

Equations (24)–(26) impose an unlimited number of LMIs that are difficult to solve. The total number of LMIs can be squeezed to a finite set using a polytopic LPV system. Using convexity, (24)–(26) will hold if it holds at the vertices of the polytope.

3.1. LPV Control for Fully Actuated Subsystem

LPV controller is devised for the fully actuated subsystem dynamics by solving the LMIs given in (24)–(26) at each vertex of the rectangular polytope using the LMI control toolbox [34].

The descriptor LPV form of altitude dynamics is

$$\begin{cases} E_z(\rho_z)\begin{bmatrix}\dot{z}\\ \ddot{z}\end{bmatrix} = \begin{bmatrix}0 & 1\\ 0 & -\dot{m}\end{bmatrix}\begin{bmatrix}z\\ \dot{z}\end{bmatrix} + B_z(\rho_z)u_4 \\ y_z = \begin{bmatrix}1 & 0\end{bmatrix}\begin{bmatrix}z\\ \dot{z}\end{bmatrix} \end{cases} \tag{28}$$

where

$$E_z(\rho_z) = \begin{bmatrix}1 & 0\\ 0 & 0\end{bmatrix} + \rho_1\begin{bmatrix}0 & 0\\ 0 & 1\end{bmatrix} + \rho_3\begin{bmatrix}0 & 0\\ 0 & 0\end{bmatrix} + \rho_4\begin{bmatrix}0 & 0\\ 0 & 0\end{bmatrix}$$

$$B_z(\rho_z) = \begin{bmatrix}0\\ -1\end{bmatrix} + \rho_3\begin{bmatrix}0\\ \frac{1}{2}\end{bmatrix} + \rho_4\begin{bmatrix}0\\ \frac{1}{2}\end{bmatrix}$$

The descriptor LPV form of yaw dynamics is

$$\begin{cases} E_\psi(\rho_\psi)\begin{bmatrix}\dot{\psi}\\ \ddot{\psi}\end{bmatrix} = \begin{bmatrix}0 & 1\\ 0 & -g_1\dot{m}\end{bmatrix}\begin{bmatrix}\psi\\ \dot{\psi}\end{bmatrix} + \begin{bmatrix}0\\ 1\end{bmatrix}U_3 \\ y_\psi = \begin{bmatrix}1 & 0\end{bmatrix}\begin{bmatrix}\psi\\ \dot{\psi}\end{bmatrix} \end{cases} \tag{29}$$

where

$$E_\psi(\rho_\psi) = \begin{bmatrix}1 & 0\\ 0 & g_2\end{bmatrix} + \rho_1\begin{bmatrix}0 & 0\\ 0 & g_1\end{bmatrix}$$

The weighting filters W_{ez} and $W_{e\psi}$ are selected as follows,

$$\left[\begin{array}{c}\dot{x}_{Wez}\\ \hline z_{1z}\end{array}\right] = \left[\begin{array}{c|c}-5.6\times10^{-6} & 0.56\\ \hline 1 & 0.5\end{array}\right]\left[\begin{array}{c}x_{Wez}\\ \hline e_z\end{array}\right] \tag{30}$$

$$\left[\begin{array}{c}\dot{x}_{We\psi}\\ \hline z_{1\psi}\end{array}\right] = \left[\begin{array}{c|c}-4.5\times10^{-4} & 0.45\\ \hline 1 & 1\end{array}\right]\left[\begin{array}{c}x_{We\psi}\\ \hline e_\psi\end{array}\right] \tag{31}$$

The static weights V_{uz} and $V_{u\psi}$ are expected to be 0.5 and 1, respectively. The static weight $d_z = 0.5$ is taken into consideration. The bounded disturbance d_r is assumed as 3.2×10^{-3} kg/s. The parameters associated with the desired LMI regions are:

$$\alpha_z = -0.5, \quad \beta_z = -30, \quad \angle\varphi_z = 50^\circ \tag{32}$$

$$\alpha_\psi = -0.5, \quad \beta_\psi = -5, \quad \angle\varphi_\psi = 50^\circ \tag{33}$$

The LPV controller gains are:

$$K_z(\rho_z) = \sum_{i=1}^{8} \alpha_{z_i} K_{z_i} \tag{34}$$

$$K_\psi(\rho_\psi) = \sum_{i=1}^{2} \alpha_{\psi_i} K_{\psi_i} \tag{35}$$

where $K_{z_i}(i = 1, 2, \ldots, 8)$ and $K_{\psi_i}(i = 1, 2)$ represent the state feedback gains, $\alpha_{z_i}(i = 1, 2, \ldots, 8)$ and $\alpha_{\psi_i}(i = 1, 2)$ represent the barycentric weights, and $\rho_z = [\rho_1, \rho_3, \rho_4]$ and $\rho_\psi = \rho_1$ are the time-varying parameters.

The robust closed-loop system stability and quadratic $\mathcal{H}_\infty$ performance γ of the LPV system are tested by using the functions *pdlstab* and *quadperf* from the MATLAB LMI Toolbox's. The LPV system will be stable, if the quantity t_{min} returned by the *pdlstab* function is negative (i.e., $t_{min} < 0$). The values achieved using the functions are given in Table 4.

Table 4. t_{min} and γ values of fully actuated subsytem.

Name	z-Position	Yaw Angle
t_{min}	−0.0512	−0.0158
γ	1.95	0.02

The quantity $t_{min} < 0$, which ensures the closed-loop system's robust stability.

3.2. LPV Control for under-Actuated Subsystem

To address the under-actuation, a multi-loop control strategy is adopted. An inner-loop LPV scheme is suggested for roll and pitch dynamics, while an outer-loop LPV strategy is proposed for the y-position and x-position dynamics to generate the roll and pitch commands. The inner-loop receives the roll and pitch commands $[\phi_{ref}, \ \theta_{ref}]$ from the outer-loop to track the desired reference positions $[y_{ref}, \ x_{ref}]$. The scheduling parameters ρ_1 and ρ_2 are not independent, which leads to conservatism. To reduce conservatism, we use a triangle polytope, BED, rather than a rectangular polytope, ABCD, as shown in Figure 9 (for details, see [35,36]).

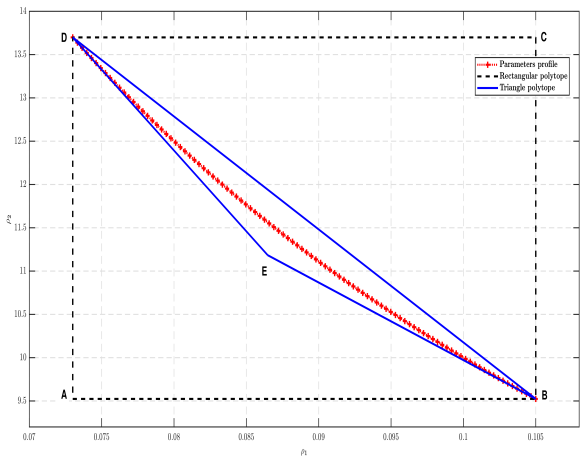

Figure 9. The structure of the Polytopes.

The roll dynamics in descriptor LPV form is

$$\begin{cases} E_\phi(\rho_\phi)\begin{bmatrix}\dot{\phi}\\ \ddot{\phi}\end{bmatrix} = A_\phi(\rho_\phi)\begin{bmatrix}\phi\\ \dot{\phi}\end{bmatrix} + B_\phi(\rho_\phi)U_1 \\ y_\phi = \begin{bmatrix}1 & 0\end{bmatrix}\begin{bmatrix}\phi\\ \dot{\phi}\end{bmatrix} \end{cases} \tag{36}$$

where

$$E_\phi(\rho_\phi) = \begin{bmatrix}1 & 0\\ 0 & e_2\end{bmatrix} + \rho_1\begin{bmatrix}0 & 0\\ 0 & e_1\end{bmatrix} + \rho_2\begin{bmatrix}0 & 0\\ 0 & e_3\end{bmatrix}$$

$$A_\phi(\rho_\phi) = \begin{bmatrix}0 & 1\\ 0 & -2e_1\dot{m}\end{bmatrix} + \rho_1\begin{bmatrix}0 & 0\\ 0 & 0\end{bmatrix} + \rho_2\begin{bmatrix}0 & 0\\ 0 & -e_2\dot{m}\end{bmatrix}$$

$$B_\phi(\rho_\phi) = \begin{bmatrix}0\\ 0\end{bmatrix} + \rho_1\begin{bmatrix}0\\ 0\end{bmatrix} + \rho_2\begin{bmatrix}0\\ 1\end{bmatrix}$$

The descriptor LPV form of pitch dynamics is

$$\begin{cases} E_\theta(\rho_\theta)\begin{bmatrix}\dot{\theta}\\ \ddot{\theta}\end{bmatrix} = A_\theta(\rho_\theta)\begin{bmatrix}\theta\\ \dot{\theta}\end{bmatrix} + B_\theta(\rho_\theta)U_2 \\ y_\theta = \begin{bmatrix}1 & 0\end{bmatrix}\begin{bmatrix}\theta\\ \dot{\theta}\end{bmatrix} \end{cases} \tag{37}$$

where

$$E_\theta(\rho_\theta) = \begin{bmatrix}1 & 0\\ 0 & f_2\end{bmatrix} + \rho_1\begin{bmatrix}0 & 0\\ 0 & f_1\end{bmatrix} + \rho_2\begin{bmatrix}0 & 0\\ 0 & f_3\end{bmatrix}$$

$$A_\theta(\rho_\theta) = \begin{bmatrix}0 & 1\\ 0 & -2f_1\dot{m}\end{bmatrix} + \rho_1\begin{bmatrix}0 & 0\\ 0 & 0\end{bmatrix} + \rho_2\begin{bmatrix}0 & 0\\ 0 & -f_2\dot{m}\end{bmatrix}$$

$$B_\theta(\rho_\theta) = \begin{bmatrix}0\\ 0\end{bmatrix} + \rho_1\begin{bmatrix}0\\ 0\end{bmatrix} + \rho_2\begin{bmatrix}0\\ 1\end{bmatrix}$$

The LPV form of x-position dynamics is

$$\begin{cases} \begin{bmatrix}\dot{x}\\ \ddot{x}\end{bmatrix} = A_x(\rho_x)\begin{bmatrix}x\\ \dot{x}\end{bmatrix} + B_x(\rho_x)u_x \\ y_x = \begin{bmatrix}1 & 0\end{bmatrix}\begin{bmatrix}x\\ \dot{x}\end{bmatrix} \end{cases} \tag{38}$$

where

$$A_x(\rho_x) = \begin{bmatrix} 0 & 1 \\ 0 & 0 \end{bmatrix} + \rho_2 \begin{bmatrix} 0 & 0 \\ 0 & -\dot{m} \end{bmatrix} + \rho_3 \begin{bmatrix} 0 & 0 \\ 0 & 0 \end{bmatrix} + \rho_4 \begin{bmatrix} 0 & 0 \\ 0 & 0 \end{bmatrix}$$

$$B_x(\rho_x) = \begin{bmatrix} 0 \\ -g \end{bmatrix} + \rho_2 \begin{bmatrix} 0 \\ 0 \end{bmatrix} + \rho_3 \begin{bmatrix} 0 \\ \frac{g}{2} \end{bmatrix} + \rho_4 \begin{bmatrix} 0 \\ \frac{g}{6} \end{bmatrix}$$

The descriptor LPV form of y-position dynamics is

$$\begin{cases} \begin{bmatrix} \dot{y} \\ \ddot{y} \end{bmatrix} = A_y(\rho_y) \begin{bmatrix} y \\ \dot{y} \end{bmatrix} + B_y(\rho_y) u_y \\ y_y = \begin{bmatrix} 1 & 0 \end{bmatrix} \begin{bmatrix} y \\ \dot{y} \end{bmatrix} \end{cases} \tag{39}$$

where

$$A_y(\rho_y) = \begin{bmatrix} 0 & 1 \\ 0 & 0 \end{bmatrix} + \rho_2 \begin{bmatrix} 0 & 0 \\ 0 & -\dot{m} \end{bmatrix} + \rho_3 \begin{bmatrix} 0 & 0 \\ 0 & 0 \end{bmatrix}$$

$$B_y(\rho_y) = \begin{bmatrix} 0 \\ g \end{bmatrix} + \rho_2 \begin{bmatrix} 0 \\ 0 \end{bmatrix} + \rho_3 \begin{bmatrix} 0 \\ -\frac{g}{6} \end{bmatrix}$$

The weight functions are chosen as:

$$\left[\begin{array}{c} \dot{x}_{We\phi} \\ \hline z_1 \end{array}\right] = \left[\begin{array}{c|c} -7.5 \times 10^{-4} & 1.936 \\ \hline 3.873 & 0.5 \end{array}\right] \left[\begin{array}{c} x_{We\phi} \\ \hline e_\phi \end{array}\right] \tag{40}$$

$$\left[\begin{array}{c} \dot{x}_{Wey} \\ \hline z_1 \end{array}\right] = \left[\begin{array}{c|c} -9.1 \times 10^{-5} & 1.045 \\ \hline 0.871 & 0.833 \end{array}\right] \left[\begin{array}{c} x_{Wey} \\ \hline e_y \end{array}\right] \tag{41}$$

Weighting filters $W_{e\psi}$, $W_{e\theta}$, W_{ex}, and W_{ey} are chosen as follows:

$$\left[\begin{array}{c} \dot{x}_{We\phi} \\ \hline z_{1\psi} \end{array}\right] = \left[\begin{array}{c|c} -7.5 \times 10^{-4} & 7.45 \\ \hline 1 & 0.5 \end{array}\right] \left[\begin{array}{c} x_{We\phi} \\ \hline e_\phi \end{array}\right] \tag{42}$$

$$\left[\begin{array}{c} \dot{x}_{We\theta} \\ \hline z_{1\theta} \end{array}\right] = \left[\begin{array}{c|c} -7.5 \times 10^{-4} & 7.45 \\ \hline 1 & 0.5 \end{array}\right] \left[\begin{array}{c} x_{We\theta} \\ \hline e_\theta \end{array}\right] \tag{43}$$

$$\left[\begin{array}{c} \dot{x}_{Wex} \\ \hline z_{1x} \end{array}\right] = \left[\begin{array}{c|c} -9.5 \times 10^{-5} & 0.95 \\ \hline 1 & 0.83 \end{array}\right] \left[\begin{array}{c} x_{Wex} \\ \hline e_x \end{array}\right] \tag{44}$$

$$\left[\begin{array}{c} \dot{x}_{Wey} \\ \hline z_{1y} \end{array}\right] = \left[\begin{array}{c|c} -9.1 \times 10^{-5} & 0.90 \\ \hline 1 & 0.83 \end{array}\right] \left[\begin{array}{c} x_{Wey} \\ \hline e_y \end{array}\right] \tag{45}$$

The values of weights $V_{u\psi} = 1$, $V_{u\theta} = 1$, $V_{ux} = \frac{\pi}{3}$, and $V_{uy} = \frac{\pi}{3}$are considered. The values of static weights $V_{dx} = 0.5$ and $V_{dy} = 0.5$ are assumed. The values of the parameters associated with the LMI regions are:

$$\alpha_\phi = -5, \quad \beta_\phi = -30, \quad \angle\varphi_\phi = 50^\circ \tag{46}$$

$$\alpha_\theta = -5, \quad \beta_\theta = -30, \quad \angle\varphi_\theta = 50^\circ \tag{47}$$

$$\alpha_x = -0.5, \quad \beta_x = -4.5, \quad \angle\varphi_x = 50^\circ \tag{48}$$

$$\alpha_y = -0.5, \quad \beta_y = -4.5, \quad \angle\varphi_y = 50^\circ \tag{49}$$

The following are the gains of the LPV controllers designed using conditions (24)–(26):

$$K_{\phi}(\rho_{\phi}) = \sum_{i=1}^{3} \alpha_{\phi i} K_{\phi i} \tag{50}$$

$$K_{\theta}(\rho_{\theta}) = \sum_{i=1}^{3} \alpha_{\theta_i} K_{\theta_i} \tag{51}$$

$$K_{x}(\rho_{x}) = \sum_{i=1}^{8} \alpha_{x_i} K_{x_i} \tag{52}$$

$$K_{y}(\rho_{y}) = \sum_{i=1}^{4} \alpha_{yi} K_{yi} \tag{53}$$

where $K_{\phi_i}(i = 1,2,3)$, $K_{\theta_i}(i = 1,2,3)$, $K_{x_i}(i = 1,2,\ldots,8)$, and $K_{y_i}(i = 1,2,\ldots,4)$ represent the state feedback gains, $\alpha_{\phi_i}(i = 1,2,3)$, $\alpha_{\theta_i}(i = 1,2,3)$, $\alpha_{x_i}(i = 1,2,\ldots,8)$, and $\alpha_{y_i}(i = 1,2,\ldots,4)$ represent the barycentric weights, and $\rho_{\phi} = [\rho_1, \rho_2]$, $\rho_{\theta} = [\rho_1, \rho_2]$, $\rho_{x} = [\rho_2, \rho_3, \rho_4]$, and $\rho_{y} = [\rho_2, \rho_3]$ are the scheduling parameters.

The values of t_{min} and γ achieved using the MATLAB functions for the under-actuated subsytem are given in Table 5.

Table 5. t_{min} and γ values of under-actuated subsytem.

Name	Roll Angle	Pitch Angle	x-Position	y-Position
t_{min}	−0.04	−0.032	−0.1042	−0.0433
γ	1.0	1.0	1.718	1.292

The quantity $t_{min} < 0$, which ensures the closed-loop system's robust stability.

4. Simulation Results and Discussion

This section presents the simulations to validate the proposed approach. The numerical simulations were carried out using the quadrotor nonlinear model represented in the Equation (9). Multiple scenarios were considered during simulations. In the first scenario, the proposed LPV algorithm was tested for reference tracking in the presence of full payload, time-varying payload, and an empty payload. Wind disturbance was applied in the second scenario, while noise was introduced to the system states in the third. Moreover, $\mathcal{H}_{\infty}$ controller with regional pole constraints was designed for the quadrotor's linear model that was obtained using small angle assumption and the average values of the mass and inertia parameters [7]. The results of the LPV scheme were compared with those attained with the LTI control design.

Case 1: The quadrotor's position is required to track a unit step signal, while the yaw angle needs to be maintained at $\angle 0^0$. The reference signals and the quadrotor's position for full payload, time-varying payload, and an empty payload are depicted in Figure 10. Figure 11 depicts the corresponding attitude angles. The control inputs and motor commands are shown in Figures 12 and 13, respectively. The tracking performance was examined in terms of system rise time (t_r), system settling time (t_s), system overshoot (OS), and system MSE. The values of the performance parameters and percentage improvements are listed in Table 6, Table 7 and Table 8, respectively. The actuator will become saturated if the motor command value is higher than 500 rad/s. Control inputs were used to calculate motor commands using (8). Effective position tracking and yaw angle stabilization were accomplished in the presence of variable mass and variable MOI using the LPV scheme as compared to the LTI controller.

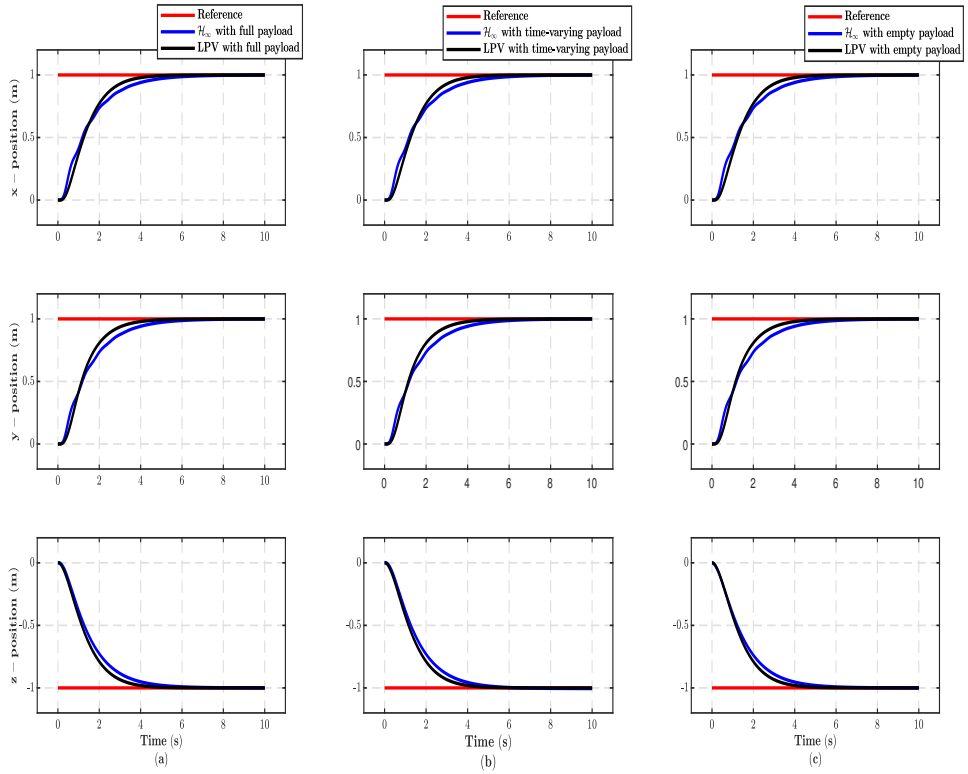

Figure 10. (**a**) The positions $[x, y, z]$ with full payload; (**b**) The positions $[x, y, z]$ with time-varying payload; (**c**) The positions $[x, y, z]$ with empty payload.

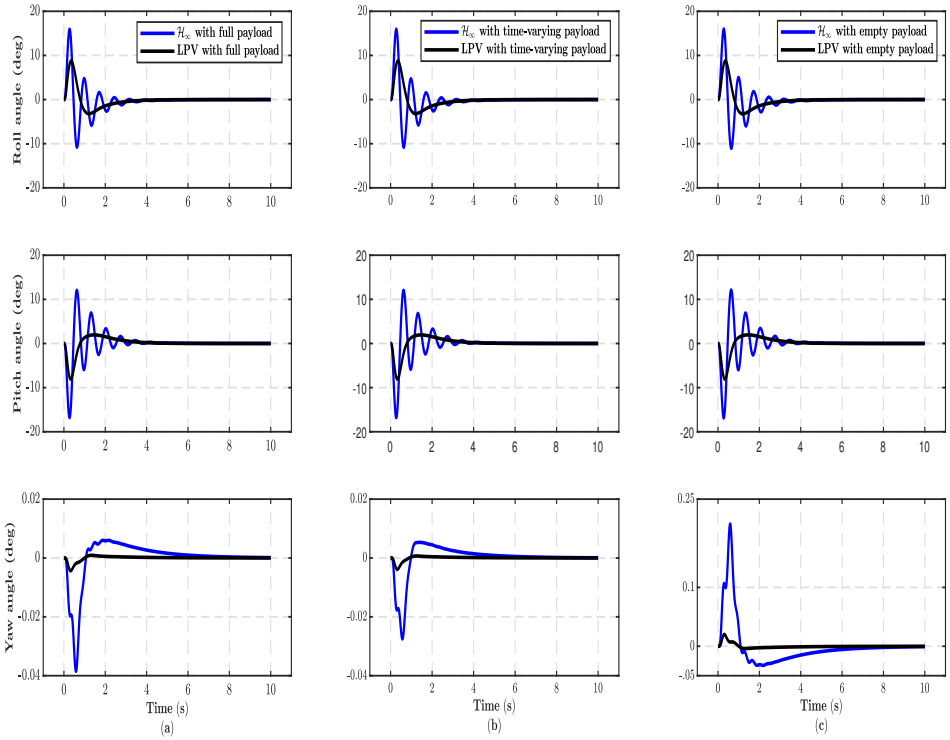

Figure 11. (**a**) The attitude angles $[\phi, \theta, \psi]$ with full payload; (**b**) The attitude angles $[\phi, \theta, \psi]$ with time-varying payload; (**c**) The attitude angles $[\phi, \theta, \psi]$ with empty payload.

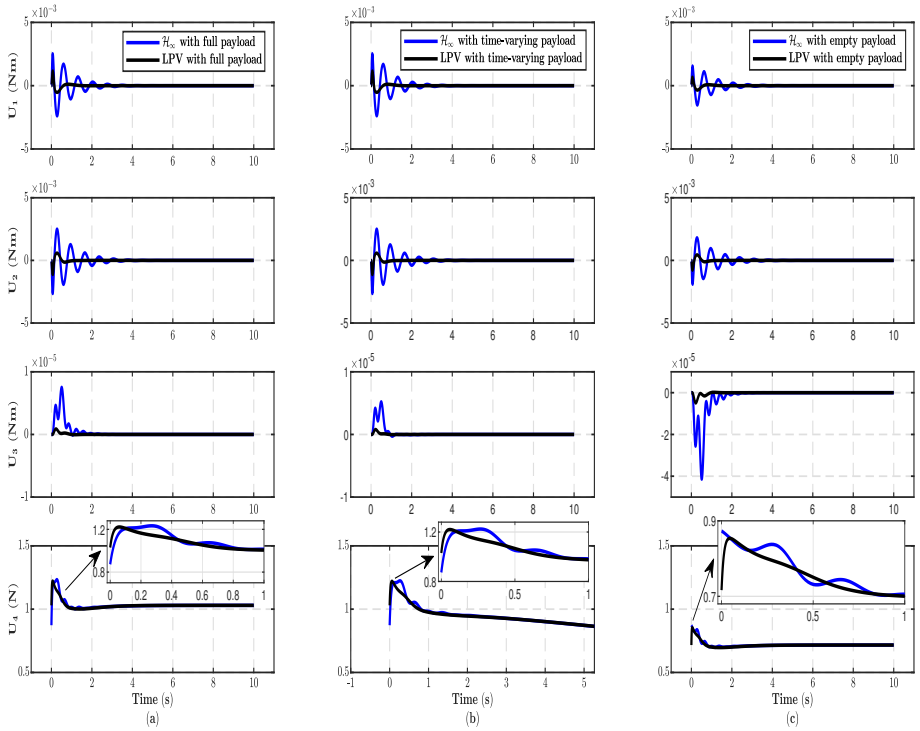

Figure 12. (**a**) The control inputs $[U_1, U_2, U_3, U_4]$ with full payload; (**b**) The control inputs $[U_1, U_2, U_3, U_4]$ with time-varying payload; (**c**) The control inputs $[U_1, U_2, U_3, U_4]$ with empty payload.

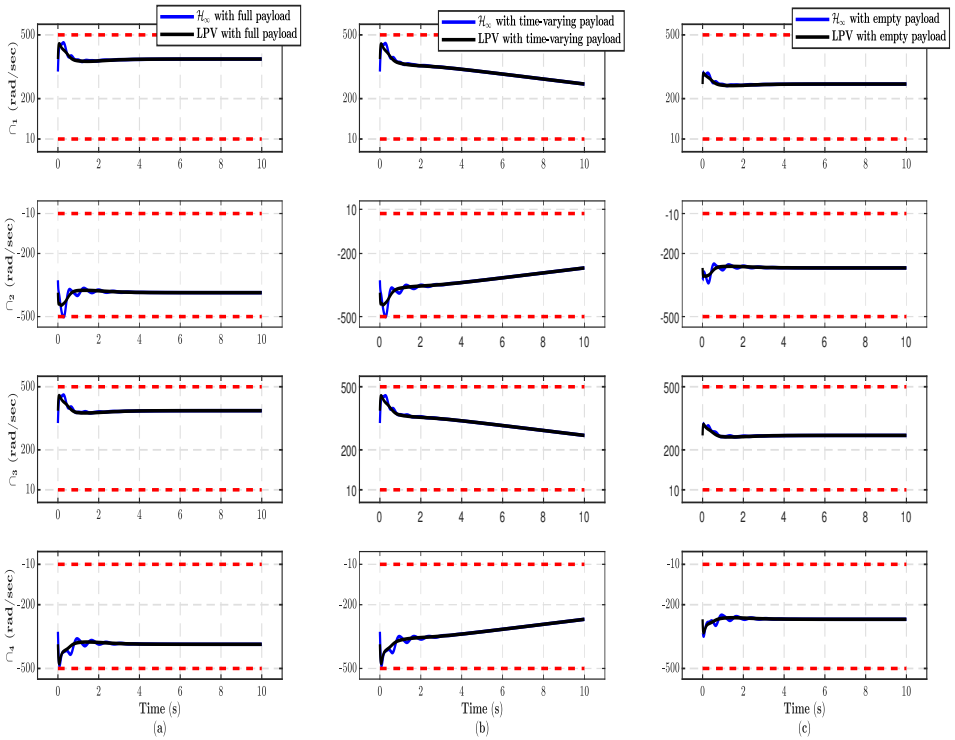

Figure 13. (**a**) The motor commands $[\cap_1, \cap_2, \cap_3, \cap_4]$ with full payload; (**b**) The motor commands $[\cap_1, \cap_2, \cap_3, \cap_4]$ with time-varying payload; (**c**) The motor commands $[\cap_1, \cap_2, \cap_3, \cap_4]$ with empty payload.

Table 6. The closed-loop performance parameters with full payload.

	Performance Parameters	LPV	$\mathcal{H}_\infty$	% Improvement
x-position	t_r	2.1954 s	2.3597 s	6.96275
	t_s	4.034 s	4.2896 s	5.9586
	OS	0%	0%	0
	MSE	0.25915 m	0.29989 m	13.585
y-position	t_r	2.0833 s	2.4246 s	14.0765
	t_s	4.0347 s	4.379 s	7.86253
	OS	0%	0%	0
	MSE	0.2507 m	0.30547 m	17.9297
z-position	t_r	2.2715 s	2.6434 s	14.069
	t_s	3.9643 s	4.61 s	14.0065
	OS	0%	0%	0
	MSE	0.238 m	0.34064 m	30.1315

Table 7. The closed-loop performance parameters with time-varying payload.

	Performance Parameters	LPV	$\mathcal{H}_\infty$	% Improvement
x-position	t_r	2.197 s	2.3653 s	7.11538
	t_s	4.0371 s	4.3168 s	6.47934
	OS	0%	0%	0
	MSE	0.24302 m	0.27943 m	13.0301
y-position	t_r	2.085 s	2.4314 s	14.2469
	t_s	4.0387 s	4.4105 s	8.42988
	OS	0%	0%	0
	MSE	0.23492 m	0.28439 m	17.3951
z-position	t_r	2.2737 s	2.6542 s	14.3358
	t_s	3.967 s	4.6502 s	14.6918
	OS	0%	0%	0
	MSE	0.22321 m	0.31365 m	28.8347

Table 8. The closed-loop performance parameters with empty payload.

	Performance Parameters	LPV	$\mathcal{H}_\infty$	% Improvement
x-position	t_r	2.1891 s	2.3288 s	5.9988
	t_s	4.021 s	4.1506 s	3.12244
	OS	0%	0%	0
	MSE	0.25374 m	0.28212 m	10.0595
y-position	t_r	2.0759 s	2.3842 s	12.931
	t_s	4.0187 s	4.2216 s	4.80623
	OS	0%	0%	0
	MSE	0.24446 m	0.2877 m	15.0295
z-position	t_r	2.2764 s	2.6105 s	12.7983
	t_s	3.9568 s	4.3802 s	9.66623
	OS	0%	0%	0
	MSE	0.23152 m	0.30689 m	24.5593

Case 2: The inertia parameters may vary due to the tilting of the quadrotor. To check the performance of the proposed control scheme in the presence of inertia parameter variation, we have considered a 20% variation in the inertia. Figure 14 depicts the variation in the water level considered over time. Figure 15 depicts the variation in the inertia with the mass. The reference signals and the quadrotor's position are depicted in Figure 16. Figure 17 depicts the corresponding attitude angles. The control inputs and motor commands are shown, respectively, in Figures 18 and 19. The simulation results indicate that the LPV scheme gives good position tracking and yaw angle stabilization in the presence of variation in the inertia parameters as compared to the LTI controller.

Case 3: To test the position tracking performance of the LPV scheme subject to dynamic payload and wind disturbance at the same time that required large tilting angle, variation in the payload was introduced at $t = 7.5$ s, and wind disturbance was applied at $t = 10$ s.

A horizontal wind model in SIMULINK was used for wind generation. A constant north-east wind speed of 5.3 m/s was assumed. The water level variation over time is shown in Figure 20. Figure 21 presents the reference signals and the position of the quadrotor. The corresponding attitude angles are shown in Figure 22. Figures 23 and 24 depict the control signals and motor commands. As can be seen, the quadrotor tracks the reference signal more effectively in the presence of time-varying payload and wind disturbance as compared to the LTI controller, which introduces significant oscillations and also results in actuator saturation as the demand for tilt angles gets higher.

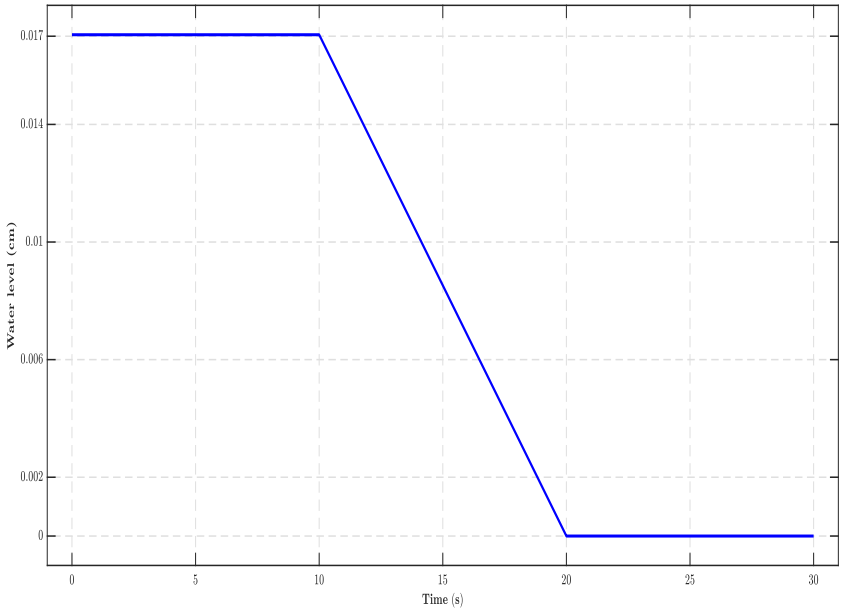

Figure 14. Variation in the water level with time.

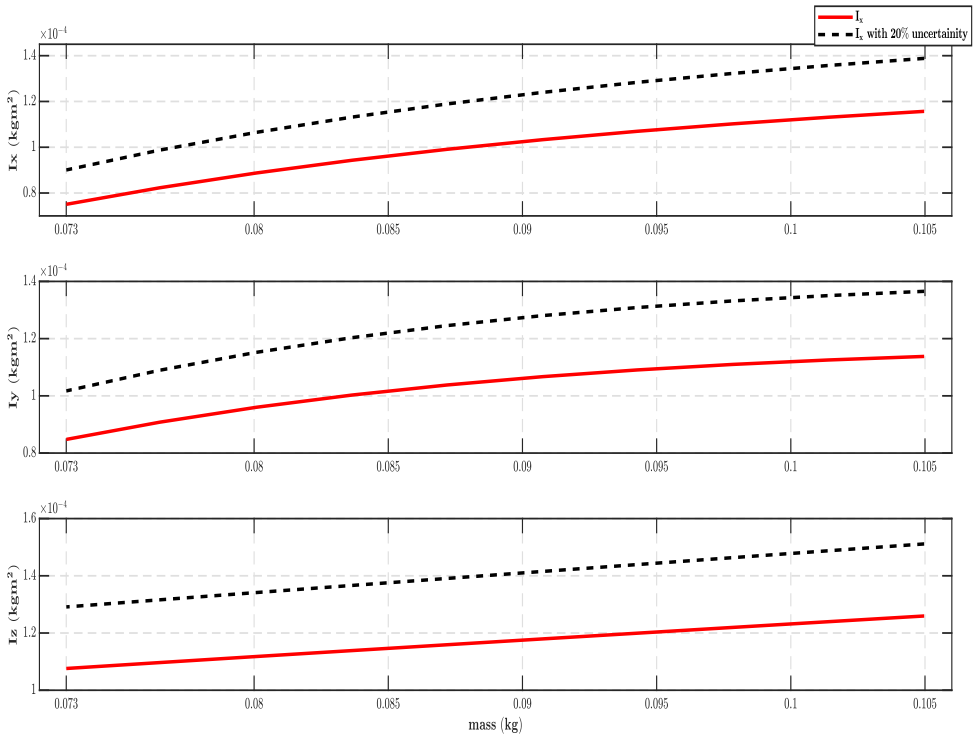

Figure 15. Variation in the inertia parameters with mass.

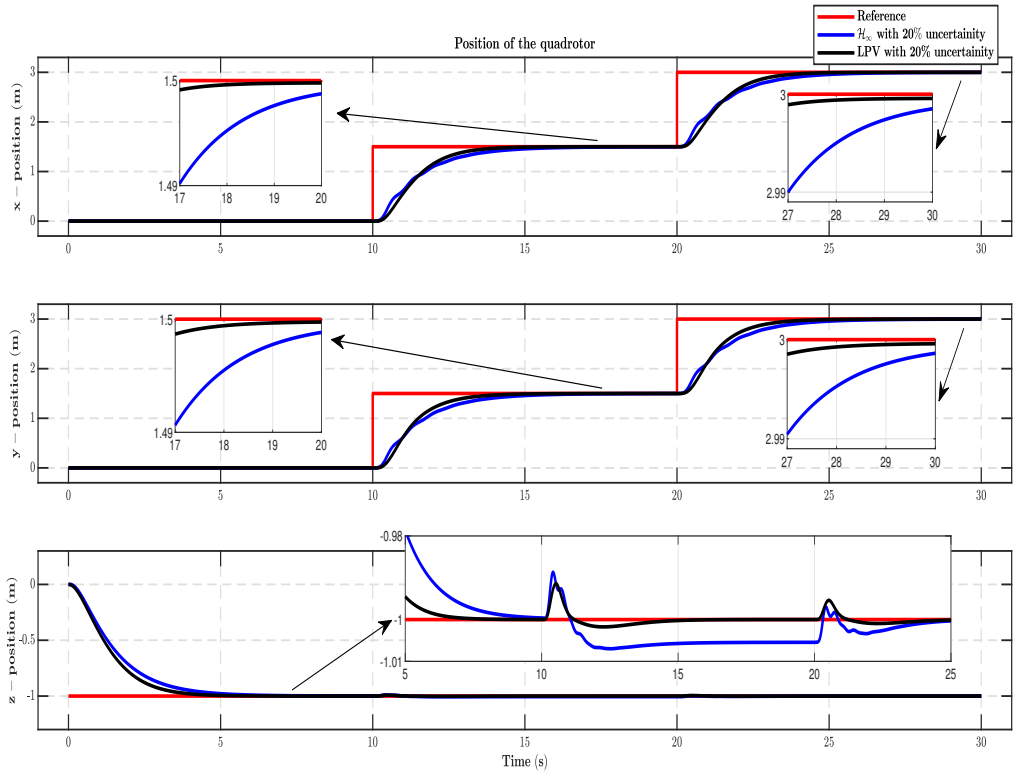

Figure 16. The positions $[x, y, z]$ with 20% variation in the inertia.

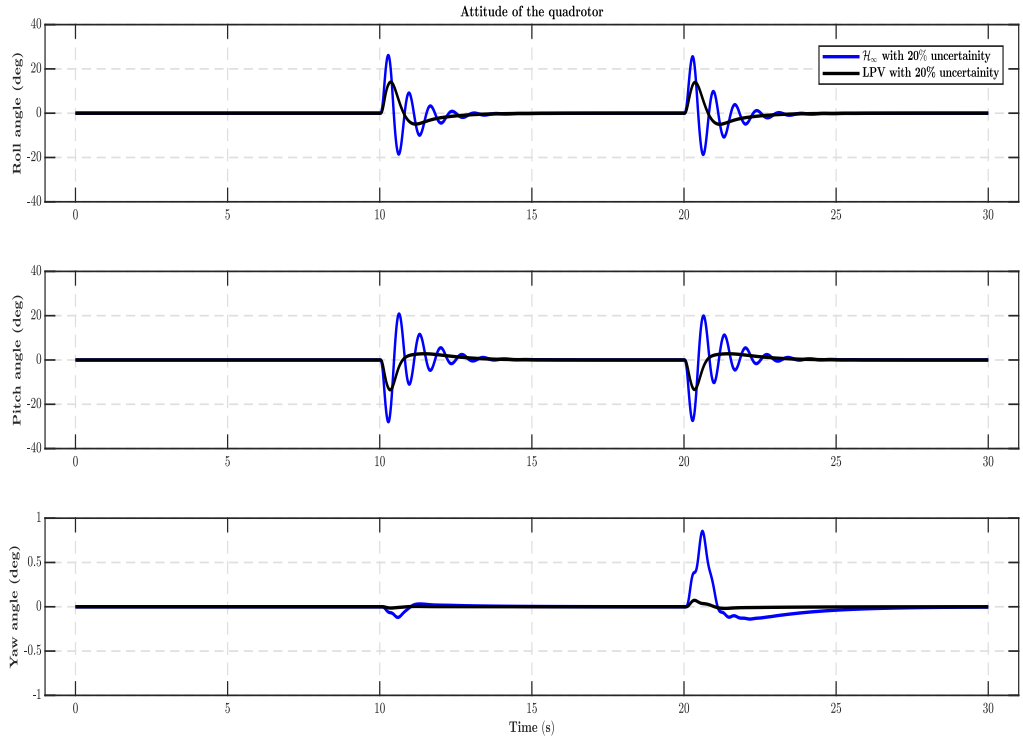

Figure 17. The attitude angles $[\phi, \theta, \psi]$ with 20% variation in the inertia.

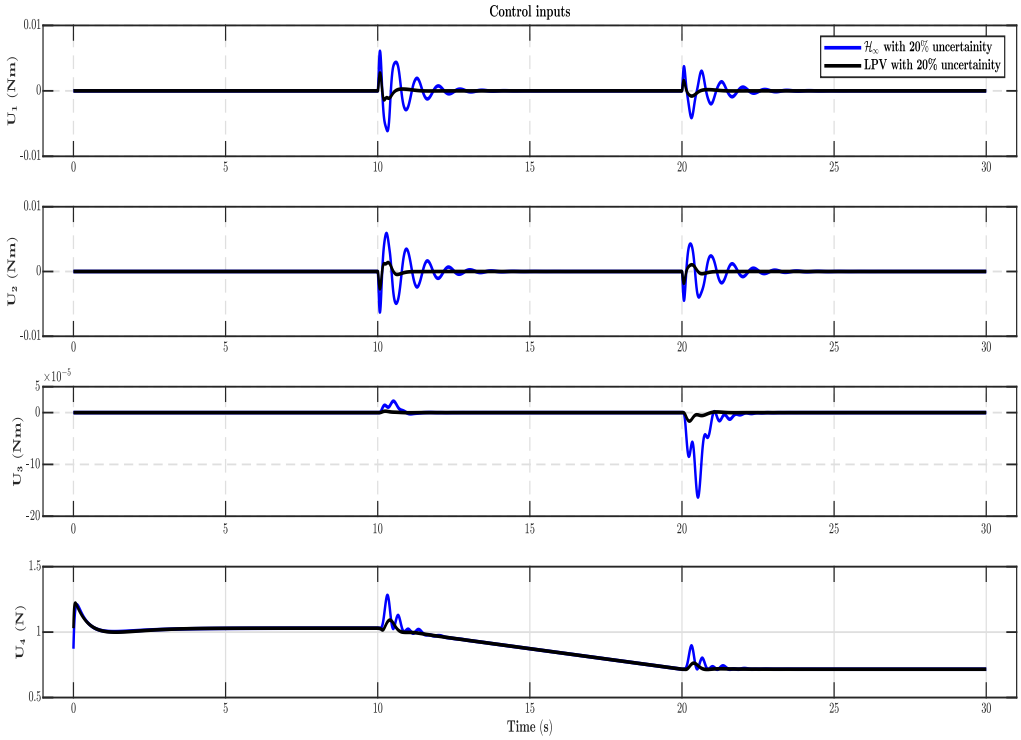

Figure 18. The control inputs $[U_1, U_2, U_3, U_4]$ with 20% variation in the inertia.

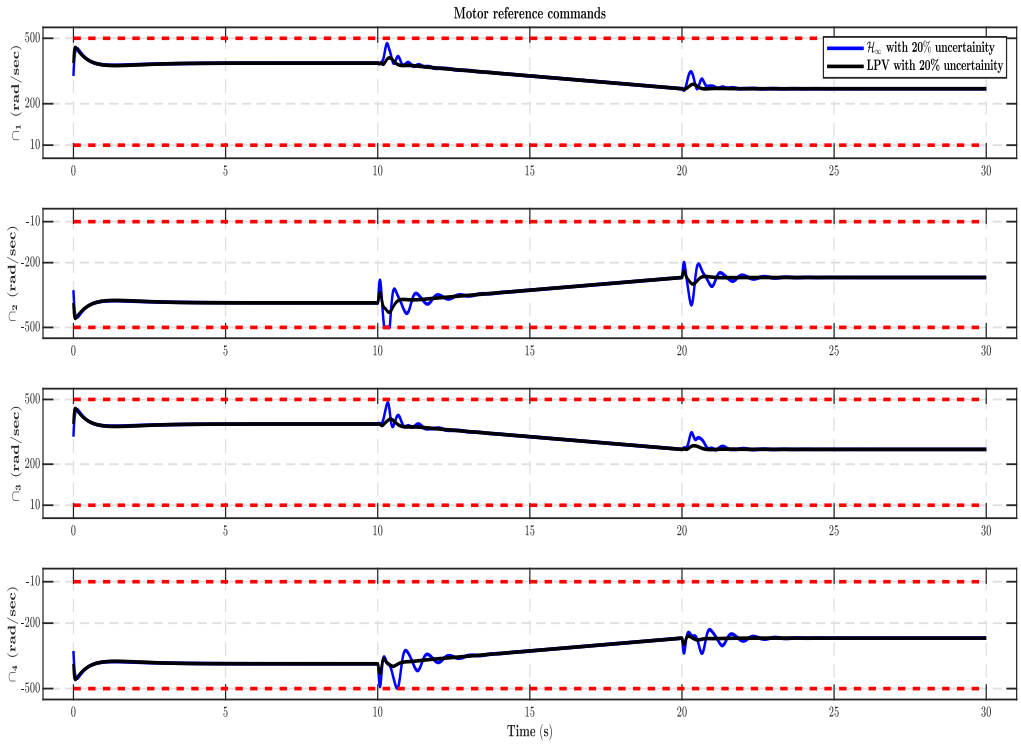

Figure 19. The motor commands $[\cap_1, \cap_2, \cap_3, \cap_4]$ with 20% variation in the inertia.

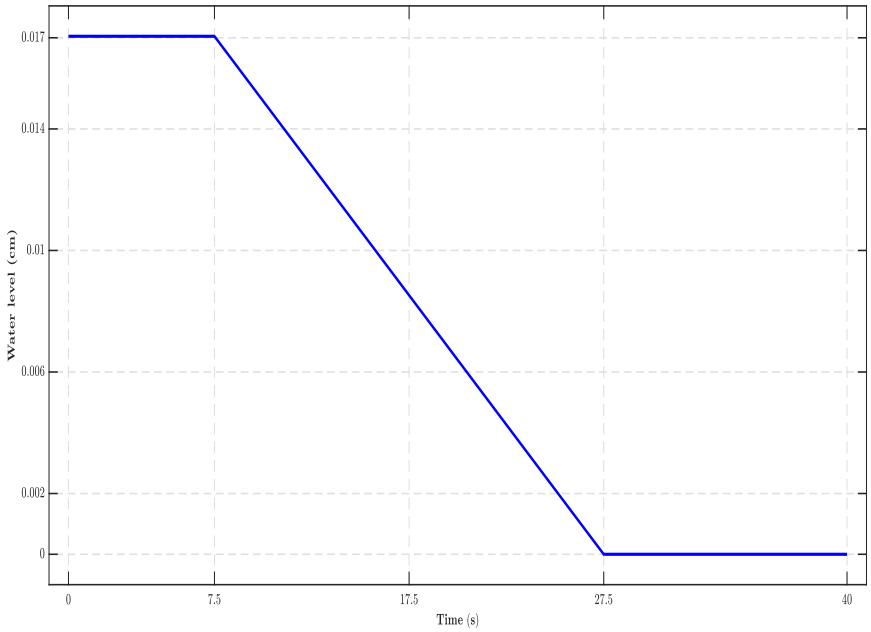

Figure 20. Variation in the water level with time.

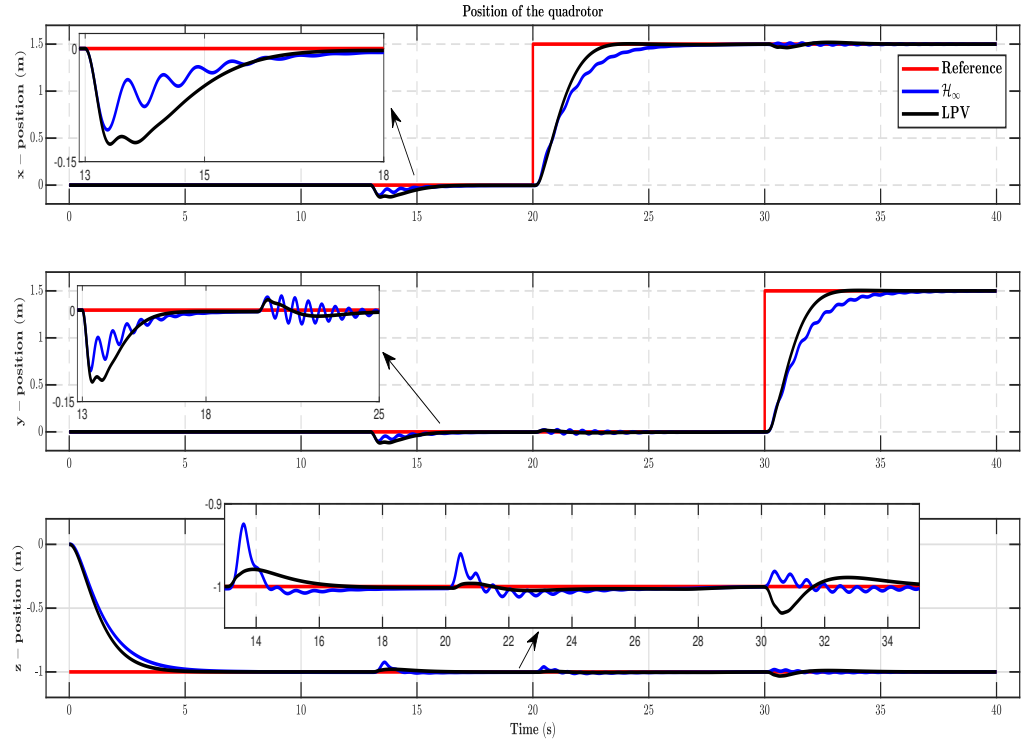

Figure 21. The positions $[x, y, z]$ with payload variation and wind disturbance.

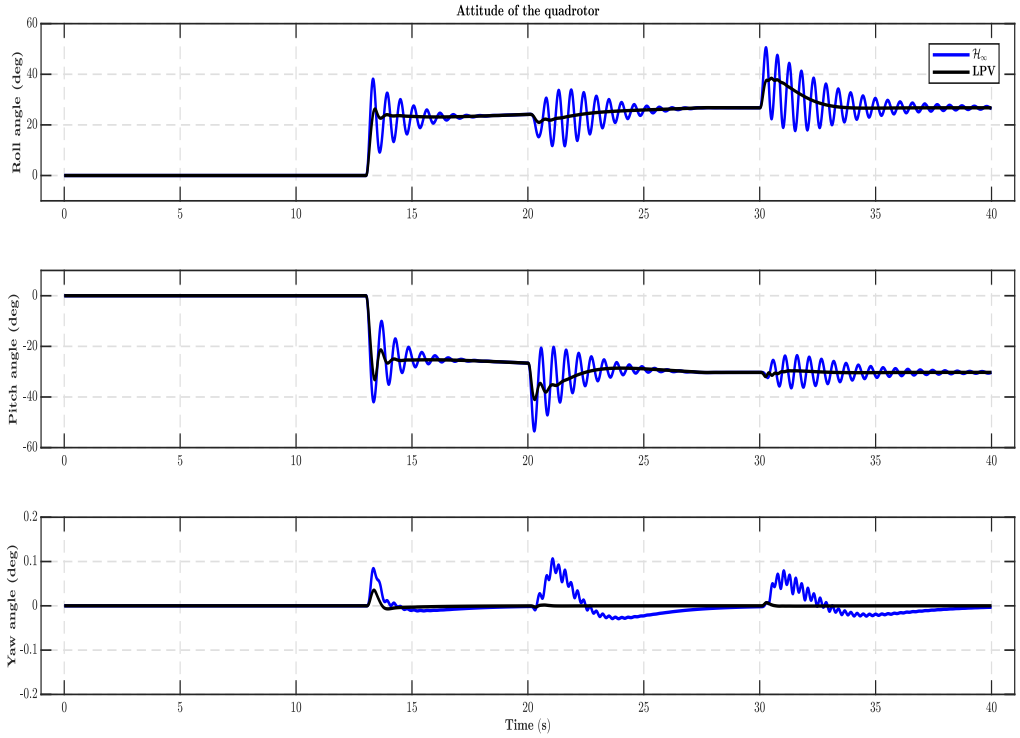

Figure 22. The attitude angles $[\phi, \theta, \psi]$ with payload variation and wind disturbance.

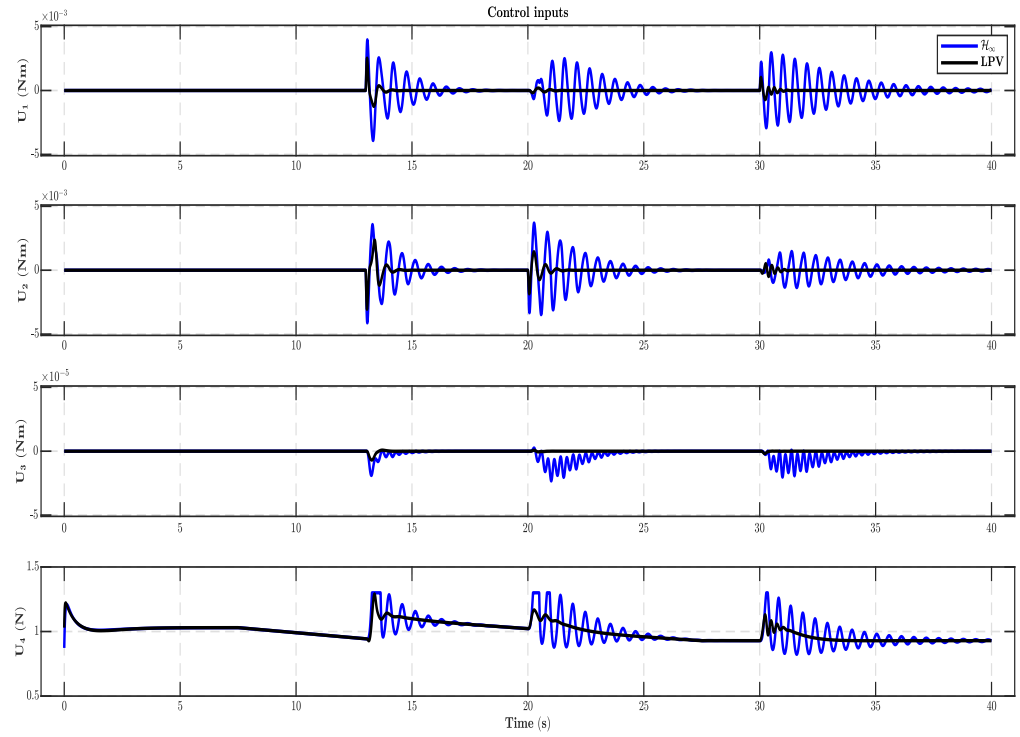

Figure 23. The control inputs $[U_1, U_2, U_3, U_4]$ with payload variation and wind disturbance.

Case 3: Gaussian noise $N(\mu, \sigma^2)$ was introduced into the quadrotor outputs in this case [37]. Noise $N(0, (1\,\text{cm})^2)$ was added to the x, y, and z positions, and Noise $N(0, (0.51°)^2)$ was introduced to the yaw, pitch, and roll angles. The water level variation over time is

shown in Figure 14. Figure 25 shows the reference signals, the position of the quadrotor, and the error plots. The attitude signals are depicted in Figure 26. Figures 27 and 28 illustrate the control signals and motor commands. The simulation results indicate that, in contrast to the LTI control scheme, the LPV design has improved tracking performance subject to dynamic mass, changing MOI, and gaussian noise.

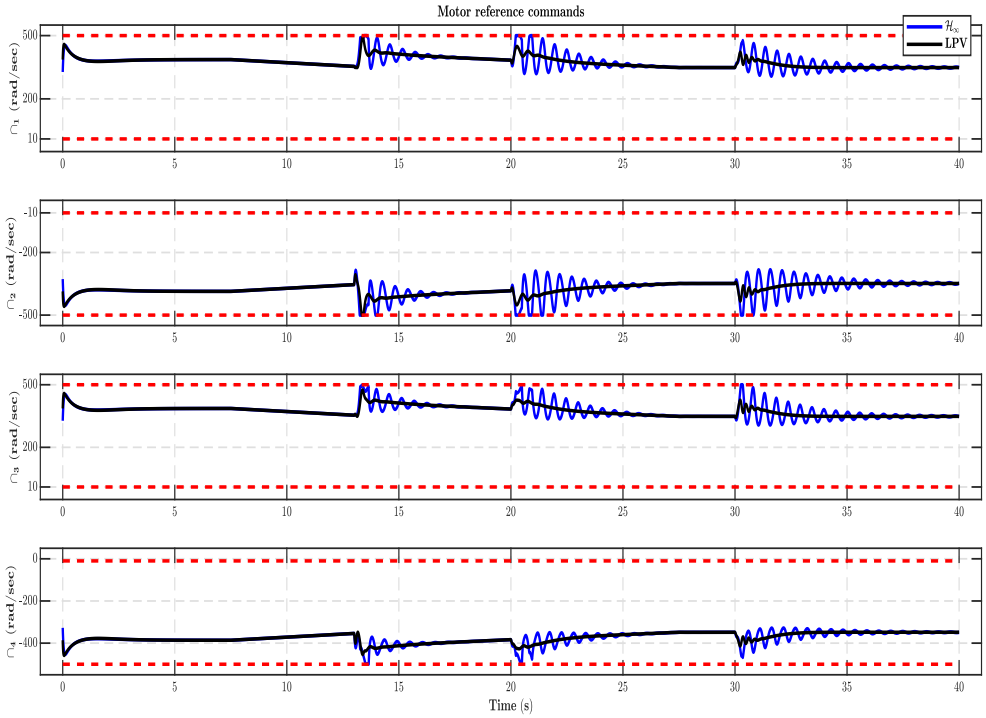

Figure 24. The motor commands $[\cap_1, \cap_2, \cap_3, \cap_4]$ with payload variation and wind disturbance.

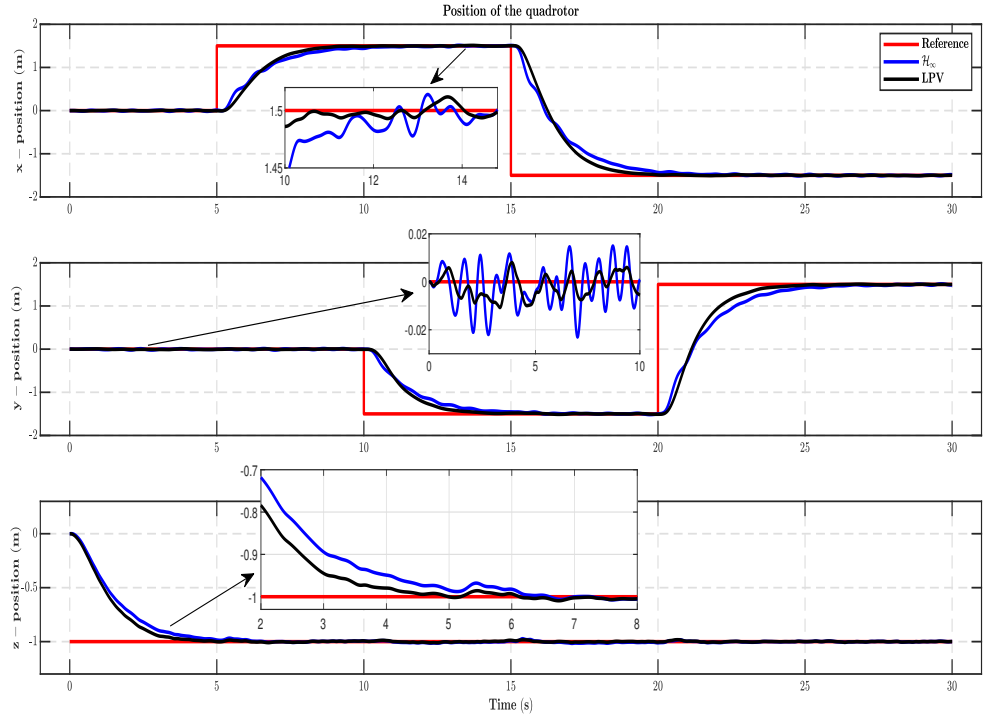

Figure 25. The positions $[x, y, z]$ with payload variation and noise.

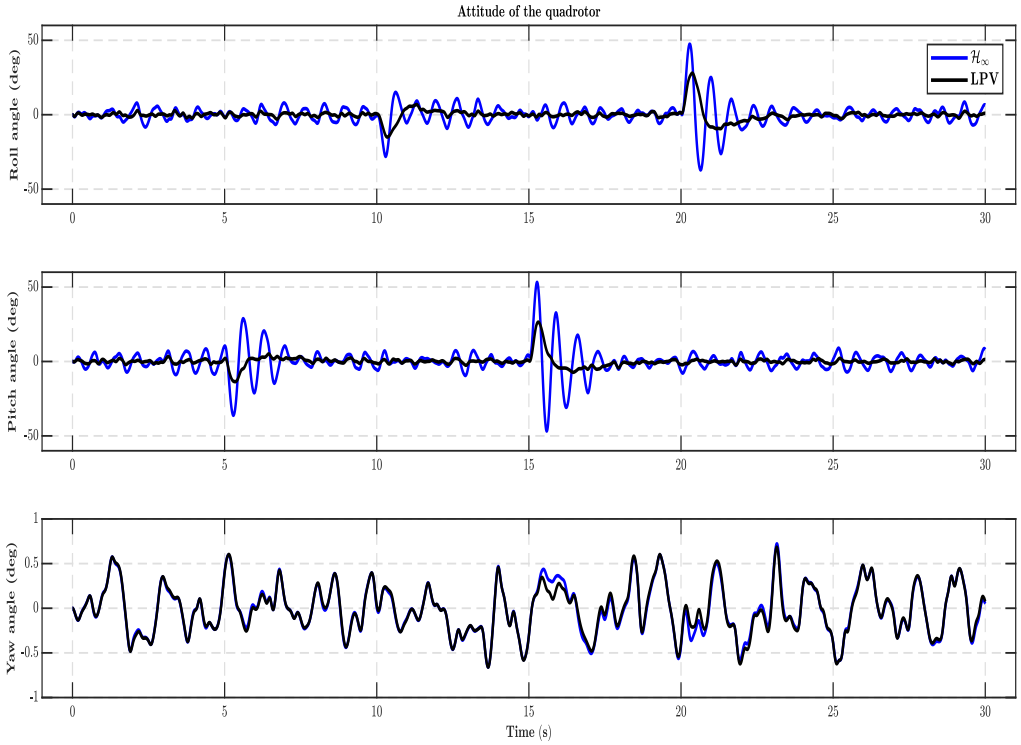

Figure 26. The attitude angles $[\phi, \theta, \psi]$ with payload variation and noise.

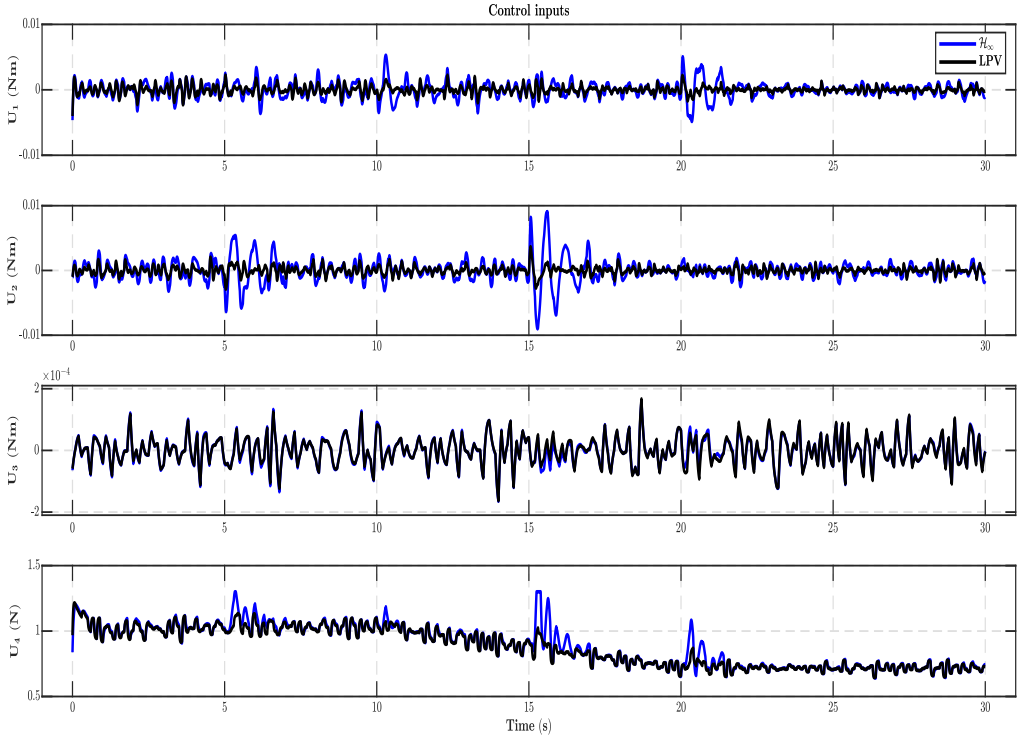

Figure 27. The control inputs $[U_1, U_2, U_3, U_4]$ with payload variation and noise.

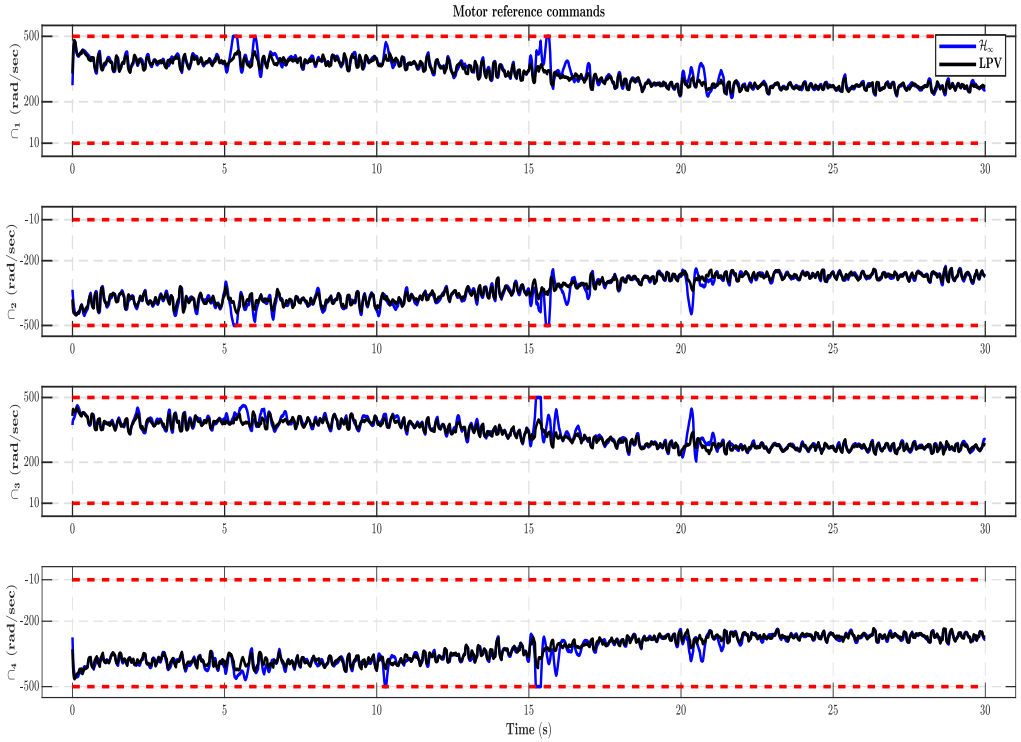

Figure 28. The motor commands $[\cap_1, \cap_2, \cap_3, \cap_4]$ with payload variation and noise.

5. Conclusions

This paper proposes an LMIs-based LPV algorithm for full motion control of a 6 DOF quadrotor model. First, an LPV model was developed for the nonlinear quadrotor model with variable payload, and then LMIs of quadratic $\mathcal{H}_\infty$ performance and D-stability were used to design the LPV control strategy. The proposed scheme was successfully evaluated in a nonlinear simulation environment. Several scenarios were simulated and studied. The outcomes of the LPV algorithm were compared with the $\mathcal{H}_\infty$ control design with pole placement constraints. The results indicate that the recommended LPV approach can achieve better position tracking in the presence of variable mass, variable inertia, mass flow rate, wind disturbance, and noise in contrast to the LTI controller. In the future, we intend to broaden our research to the hardware implementation of the suggested control scheme in order to assess its stability, robustness, and effectiveness.

Author Contributions: Conceptualization, A.S., A.I.B. and F.M.M.; Methodology, A.S., A.I.B. and F.M.M.; Software, A.S.; Validation, A.S.; Formal analysis, A.S.; Investigation, A.S.; data curation, A.S.; writing—original draft preparation, A.S.; writing—review and editing, A.S., A.I.B. and F.M.M.; Visualization, A.S.; Supervision, A.I.B. and F.M.M. All authors have read and agreed to the published version of the manuscript.

Funding: This research received no external funding.

Institutional Review Board Statement: Not applicable.

Informed Consent Statement: Not applicable.

Data Availability Statement: Not applicable.

Conflicts of Interest: The authors declare no conflict of interest.

References

1. Li, Y.; Song, S. A survey of control algorithms for quadrotor unmanned helicopter. In Proceedings of the IEEE 5th International Conference on Advanced Computational Intelligence (ICACI), Nanjing, China, 18–20 October 2012; pp. 365–369.
2. Maaruf, M.; Mahmoud, M.S.; Ma'arif, A. A survey of control methods for quadrotor uav. *Int. J. Robot. Control Syst.* **2022**, *2*, 652–665.
3. Shaw, K.K.; Vimalkumar, R. Design and development of a drone for spraying pesticides, fertilizers and disinfectants. *Eng. Res. Technol. (IJERT)* **2020**, *9*, 1181–1185.
4. Hanif, A.S.; Han, X.; Yu, S.H. Independent Control Spraying System for UAV-Based Precise Variable Sprayer: A Review. *Drones* **2022**, *6*, 383.
5. Li, J.; Li, Y. Dynamic analysis and PID control for a quadrotor. In Proceedings of the 2011 IEEE International Conference on Mechatronics and Automation, Beijing, China, 7–10 August 2011; pp. 573–578.
6. Dong, W.; Gu, G.Y.; Zhu, X.; Ding, H. Modeling and control of a quadrotor UAV with aerodynamic concepts. *World Acad. Sci. Eng. Technol.* **2013**, *7*, 901–906.
7. Martins, L.; Cardeira, C.; Oliveira, P. Linear quadratic regulator for trajectory tracking of a quadrotor. *IFAC-PapersOnLine* **2019**, *52*, 176–181.
8. Mokhtari, A.; Benallegue, A.; Daachi, B. Robust feedback linearization and GH/sub/spl infin//controller for a quadrotor unmanned aerial vehicle. In Proceedings of the 2005 IEEE/RSJ International Conference on Intelligent Robots and Systems, Edmonton, AB, Canada, 2–6 August 2005; pp. 1198–1203.
9. Araar, O.; Aouf, N. Full linear control of a quadrotor UAV, LQ vs H_∞. In Proceedings of the 2014 UKACC International Conference on Control (CONTROL), Loughborough, UK, 9–11 July 2014; pp. 133–138.
10. Rangajeeva, S.L.; Whidborne, J.F. Linear parameter varying control of a quadrotor. In Proceedings of the 2011 6th International Conference on Industrial and Information Systems, Kandy, Sri Lanka, 16–19 August 2011; pp. 483–488.
11. Cisneros, P.S.; Hoffmann, C.; Bartels, M.; Werner, H. Linear parameter-varying controller design for a nonlinear quad-rotor helicopter model for high speed trajectory tracking. In Proceedings of the 2016 American Control Conference (ACC), Boston, MA, USA, 6–8 July 2016; pp. 486–491.
12. Nie, L.; Cai, B.; Lu, S.; Qin, H.; Zhang, L. Finite-time switched LPV control of quadrotors with guaranteed performance. *J. Frankl. Inst.* **2021**, *358*, 7032–7054.
13. Pham, T.H.; Mammar, S. Quadrotor lpv control using static output feedback. In Proceedings of the 2019 IEEE 16th International Conference on Networking, Sensing and Control (ICNSC), Banff, AB, Canada, 9–11 May 2019; pp. 74–79.
14. Pham, T.H.; Ichalal, D.; Mammar, S. LPV and Nonlinear-based control of an Autonomous Quadrotor under variations of mass and moments of inertia. *IFAC-PapersOnLine* **2019**, *52*, 176–183.
15. Pham, T.H.; Ichalal, D.; Mammar, S. Lpv state-feedback controller for attitude/altitude stabilization of a mass-varying Quadrotor. In Proceedings of the 2020 20th International Conference on Control, Automation and Systems (ICCAS), Busan, Republic of Korea, 13–16 October 2020; pp. 212–218.
16. Nie, L.; Cai, B.; Zhu, Y.; Yang, J.; Zhang, L. Switched linear parameter-varying tracking control for quadrotors with large attitude angles and time-varying inertia. *Optim. Control Appl. Methods* **2021**, *42*, 1320–1336.
17. Sierra, J.E.; Santos, M. Wind and payload disturbance rejection control based on adaptive neural estimators: Application on quadrotors. *Complexity* **2019**, *2019*, 6460156.
18. Vahdanipour, M.; Khodabandeh, M. Adaptive fractional order sliding mode control for a quadrotor with a varying load. *Aerosp. Sci. Technol.* **2019**, *86*, 737–747.
19. Zhao, J.; Ding, X.; Jiang, B.; Jiang, G.; Xie, F. A novel control strategy for quadrotors with variable mass and external disturbance. *Int. J. Robust Nonlinear Control* **2021**, *31*, 8605–8631.
20. Lee, J.W.; Xuan-Mung, N.; Nguyen, N.P.; Hong, S.K. Adaptive altitude flight control of quadcopter under ground effect and time-varying load: Theory and experiments. *J. Vib. Control* **2023**, *29*, 571–581.
21. Wu, X.; Xiao, B.; Qu, Y. Modeling and sliding mode-based attitude tracking control of a quadrotor UAV with time-varying mass. *ISA Trans.* **2019**, *124*, 436–443.
22. Yang, P.; Wang, Z.; Zhang, Z.; Hu, X. Sliding Mode Fault Tolerant Control for a Quadrotor with Varying Load and Actuator Fault. *Actuators* **2021**, *10*, 323.
23. Kun, D.W.; Hwang, I. Linear matrix inequality-based nonlinear adaptive robust control of quadrotor. *J. Guid. Control Dyn.* **2016**, *39*, 996–1008.
24. Okasha, M.; Kralev, J.; Islam, M. Design and Experimental Comparison of PID, LQR and MPC Stabilizing Controllers for Parrot Mambo Mini-Drone. *Aerospace* **2022**, *9*, 298
25. Noordin, A.; Basri, M.A.M.; Mohamed, Z. Simulation and experimental study on PID control of a quadrotor MAV with perturbation. *Bull. Electr. Eng. Inform.* **2020**, *9*, 1811–1818.
26. Apkarian, P. Lmi techniqes in control engineering from theory to practice. In Proceedings of the IEEE Conference on Decision and Control (IEEE CDC'96 Workshop), Kobe, Japan, 11–13 December 1996.
27. Han, J.; Liu, X.; Wei, X.; Sun, S. A dynamic proportional-integral observer-based nonlinear fault-tolerant controller design for nonlinear system with partially unknown dynamic. *IEEE Trans. Syst. Man Cybern. Syst.* **2021**, *52*, 5092–5104.
28. Apkarian, P.; Gahinet, P.; Becker, G. Self-scheduled H_∞ control of linear parameter-varying systems: A design example. *Automatica* **1995**, *31*, 1251–1261.

29. Zollars, M.D.; Cobb, R.G.; Grymin, D.J. Optimal path planning for suas waypoint following in urban environments. In Proceedings of the 2018 IEEE Aerospace Conference, Big Sky, MT, USA, 3–10 March 2018; pp. 1–8.
30. Theis, J.; Pfifer, H. Observer-based synthesis of linear parameter-varying mixed sensitivity controllers. *Int. J. Robust Nonlinear Control* **2020**, *30*, 5021–5039.
31. Liu, Y.; Jiang, C. Mixed-Sensitivity Control for Drag-Free Spacecraft Based on state space. *Aerospace* **2022**, *9*, 708.
32. Chilali, M.; Gahinet, P. H/sub/spl infin//design with pole placement constraints: An lmi approach. *IEEE Trans. Autom. Control* **1996**, *41*, 358–367.
33. Chilali, M.; Gahinet, P.; Apkarian, P. Robust pole placement in LMI regions. *IEEE Trans. Autom. Control* **1999**, *44*, 2257–2270.
34. Gahinet, P.; Nemirovskii, A.; Laub, A.J.; Chilali, M. The lmi control toolbox. In Proceedings of 1994 33rd IEEE Conference on Decision and Control, Lake Buena Vista, FL, USA, 14–16 December 1994; Volume 3, pp. 2038–2041.
35. Wada, N.; Takahashi, A.; Saeki, M.; Nishimura, M. Vehicle yaw control using an active front steering system with measurements of lateral tire forces. In *The Abstracts of the International Conference on Advanced Mechatronics: Toward Evolutionary Fusion of IT and Mechatronics (ICAM 2010.5)*; The Japan Society of Mechanical Engineers: Tokyo, Japan, 2010; pp. 319–324.
36. Li, P.; Nguyen, A.T.; Du, H.; Wang, Y.; Zhang, H. Polytopic LPV approaches for intelligent automotive systems: State of the art and future challenges. *Mech. Syst. Signal Process.* **2021**, *161*, 107931.
37. Trapiello, C.; Puig, V.; Morcego, B. Position-heading quadrotor control using LPV techniques. *IET Control Theory Appl.* **2019**, *13*, 783–794.